






# Feeding decision-making by a single neuron via disparate neurotransmitters

Received: 24 March 2025

Accepted: 2 February 2026

Published online: 13 February 2026

 Check for updates

Doruk Savaş <sup>1,2,4</sup>, Angel M. Okoro<sup>1,2</sup>, Rareş A. Moşneanu<sup>1,2</sup>, Anthony M. Crown<sup>1,2,5</sup>, Zeyu Chang <sup>3</sup>, Rebecca Siegel<sup>1,2,6</sup>, Altar Sorkaç <sup>1,2</sup>, Meet Zandawala <sup>1,2,7</sup> & Gilad Barnea <sup>1,2</sup> 

Animals use gustatory information to decide whether to ingest nutritious substances or avoid toxic ones. Although certain neurons in the gustatory circuits respond to both aversive and appetitive signals, how these neurons resolve inputs with opposing valences is unknown. Here, we examine how the *Drosophila melanogaster* neuropeptide leucokinin (LK) affects gustatory information processing to elicit the appropriate feeding behaviors. We identify the subesophageal LK neurons (SELKs) as downstream synaptic partners of gustatory receptor neurons and show that these two groups are functionally connected. We then show that SELKs affect bitter avoidance through LK release and food intake in an acetylcholine-dependent manner. Our study uncovers a mechanism whereby strong activation of SELKs results in LK release, leading to feeding suppression, while weak activation results in acetylcholine-dependent feeding promotion. Thus, our results reveal that a single pair of neurons, SELKs, differentially controls opposing feeding behaviors via distinct neurotransmitters.

To survive, animals must make feeding-related decisions based on the quality of the available food and their internal states. In these decisions, they use the sense of taste to discern nutritious, palatable substances, which are ingested, from potentially toxic ones, which are rejected<sup>1</sup>. In *Drosophila melanogaster*, gustatory receptor neurons (GRNs) are found in the peripheral taste organs, such as proboscis labella, leg tarsi, and pharynx. GRNs express gustatory receptors that sense non-volatile chemicals in the environment and send information about the quality of a potential food source to the central nervous system<sup>2–4</sup>. Sweet and bitter tastants are sensed by distinct gustatory receptors that are expressed by functionally segregated GRNs that drive opposing feeding behaviors<sup>5</sup>: while activation of sweet-sensing GRNs promotes feeding<sup>6,7</sup>, activation of bitter-sensing GRNs leads to food aversion<sup>8–11</sup>. GRNs primarily relay taste information to the

subesophageal zone (SEZ), the primary gustatory processing center in the brain that harbors sensorimotor circuits for feeding<sup>12</sup>.

The control of feeding requires complex sensorimotor processing that, even in its simplest form, involves multiple layers of interneurons between the sensory and motor neuron populations<sup>13</sup>. Further, although sweet and bitter GRNs exhibit non-overlapping arborizations in the SEZ<sup>14,15</sup>, the anatomical organization of the SEZ is considerably less structured than the highly structured glomerular arrangement of the olfactory system or the layered architecture of the visual system.

Given the more diffuse organization of the SEZ, it is conceivable that some interneurons would receive overlapping inputs from circuits encoding disparate taste modalities. Indeed, electrophysiological and calcium imaging experiments in both mammals and insects reveal that taste representation in the second-order gustatory neurons is complex,

<sup>1</sup>Department of Neuroscience, Brown University, Providence, RI, USA. <sup>2</sup>Carney Institute for Brain Science, Brown University, Providence, RI, USA. <sup>3</sup>Department of Biochemistry, Molecular Biology and Biotechnology, University of Nevada, Reno, NV, USA. <sup>4</sup>Present address: Howard Hughes Medical Institute, Harvard Medical School, Boston, MA, USA. <sup>5</sup>Present address: Princeton Neuroscience Institute, Princeton University, Princeton, NJ, USA. <sup>6</sup>Present address: Grossman School of Medicine, New York University, New York, NY, USA. <sup>7</sup>Present address: Department of Biochemistry, Molecular Biology and Biotechnology, University of Nevada, Reno, NV, USA. ✉e-mail: [gilad\\_barnea@brown.edu](mailto:gilad_barnea@brown.edu)

as some of these neurons respond to taste modalities with opposing valences (i.e., sweet and bitter)<sup>16–20</sup>.

One mechanism by which the complex representation of taste information in the SEZ can be resolved to instruct proper feeding behaviors is through neuromodulation. Indeed, various neuromodulatory systems integrate the metabolic needs and internal state of the animal with external stimuli, such as taste, to regulate feeding<sup>21</sup>. Some neuromodulatory systems involve the use of neuropeptides that bind their cognate receptors on target neurons and thereby alter their intrinsic properties<sup>22,23</sup>. Neuropeptides regulate a wide range of physiological states, such as hunger, thirst, and sleep<sup>24–28</sup>. Seminal studies in the crustacean stomatogastric ganglion revealed how an intricate network of neuromodulatory systems affects the sensory-motor transformation to alter circuit dynamics and behavioral output<sup>22,29</sup>. Notably, these studies showed that neurons in the ganglion employ cotransmission of neurotransmitters and neuropeptides<sup>22</sup>.

Cotransmission is a process by which neurons use more than one neurotransmitter, or neuropeptide, to communicate with their downstream targets. In this manner, a single neuron can generate diverse functional outputs that are superimposed on its synaptic connections<sup>22,23,30</sup>. The differential release of these neurotransmitters can be ensured through spatial segregation of the vesicles, stimulus intensity, or differential Ca<sup>++</sup> sensitivity<sup>31</sup>. The capacity of a single neuron to release two orthogonal chemical signals could endow it with the ability to govern two separate behaviors in a context-dependent manner. While such neurons have been reported in various models<sup>30,32</sup>, how they produce the appropriate behavioral outcomes in response to various inputs remains elusive. Hence, we sought to characterize the neuromodulators in the SEZ to understand how they shape the sensorimotor transformations that underlie feeding behaviors.

## Results

### SELKs are postsynaptic to both sweet and bitter GRNs

The SEZ circuits for taste processing, which compute feeding decisions based on the quality of food, are complex and highly interconnected. Lessons learned from studying the stomatogastric ganglion in crabs and lobsters indicate that a single ensemble of a few neurons can regulate diverse functions through the coordinated release of various neuromodulators<sup>22,23</sup>. Thus, we wished to examine whether neuropeptidergic neurons receiving input from the SEZ shape feeding decisions based on taste information from the GRNs in flies. To identify a candidate neuropeptide that could serve this function, we conducted an anatomical screen in which we initiated *trans*-Tango, a genetically encoded anterograde transsynaptic labeling technique<sup>33</sup>, from bitter or sweet GRNs and co-stained the brains for the postsynaptic marker and various neuropeptides (Supplementary Information Table). To facilitate the identification of the postsynaptic neurons, we used a configuration of *trans*-Tango with a nuclear red fluorescent protein as its output<sup>34</sup>.

Our anatomical screen revealed a pair of postsynaptic partners of GRNs residing in ventral SEZ and marked by the antibody against the neuropeptide LK (Fig. 1a, b). The invertebrate neuropeptide LK has emerged as a key regulator of diverse metabolic processes, including feeding<sup>35</sup>, as flies in which LK expression is perturbed demonstrate feeding deficiencies<sup>36–38</sup>. Four groups of LK neurons in *Drosophila* are classified based upon their anatomical location<sup>39</sup>, and each group has distinct functions ranging from regulation of feeding and sleep<sup>24,25,28</sup> to water homeostasis<sup>36,40,41</sup>. The pair of SEZ LK neurons identified in our screen is termed SELKs. They elaborate extensive arborizations in the SEZ where they run along the midline and branch laterally. The SELKs also project to the ventral nerve cord<sup>39</sup>. Due to their extensive innervation in the SEZ, SELKs are thought to affect gustatory information processing<sup>42</sup>. However, the role of SELKs in feeding is unknown.

Notably, our anatomical analysis indicates that SELKs receive input from both bitter-sensing Gr66a<sup>+</sup> GRNs (Fig. 1a) and sweet-sensing Gr64f<sup>+</sup> GRNs (Fig. 1b). Further, our analysis revealed that SELKs receive

input from GRNs residing in anatomically distinct taste organs: the proboscis labella, leg tarsi, and pharynx (Supplementary Fig. 1a–c). We found that no other LK neuron was postsynaptic to GRNs from either modality except for a few abdominal ganglion LK neurons (Supplementary Fig. 1d–g). We did not observe any colocalization of the postsynaptic marker and LK antibodies in the absence of a genetic driver (Supplementary Fig. 1h). These results indicate that SELKs are the only LK neurons in the central brain that are postsynaptic to both bitter- and sweet-sensing GRNs.

To corroborate these findings, we compared them to the electron microscopy (EM) reconstruction of a fly brain connectome<sup>43</sup>. To this end, we used the mosaic labeling approach SPARC<sup>44</sup> to visualize a single SELK. This analysis revealed that SELKs predominantly project to the contralateral brain hemisphere and arborize in the dorsal SEZ (Supplementary Fig. 2a). Using this image as a guide, we identified both SELKs (Supplementary Fig. 2b) in the connectome (cell type: DNg68; body IDs: 720575940629543409 and 720575940630808827). Notably, the connectome annotation predicts that SELKs use acetylcholine (ACh) as a fast-acting neurotransmitter, with prediction scores of 0.59 and 0.66.

We next queried the presynaptic partners of SELKs in a fly connectome<sup>43,45–47</sup>. Our connectome analysis revealed that SELKs receive the majority of their synaptic inputs from ascending and central neurons (42% and 41% of all their inputs, respectively; Supplementary Fig. 2c). Only 2% of all their synaptic inputs are from 46 sensory neurons (Supplementary Fig. 2c). The majority of these sensory neurons are GRNs (37 neurons); 13 of which are bitter GRNs, additional 13 are sweet/water GRNs, and 11 are pharyngeal GRNs. Among the gustatory neurons, the pharyngeal GRNs make the largest number of synapses with SELKs (Supplementary Fig. 2d–f).

We then sought to investigate the functional connectivity between GRNs and SELKs. To this end, we expressed the optogenetic activator CsChrimson<sup>48</sup> in bitter or sweet GRNs, and the calcium indicator GCaMP6s<sup>49</sup> in LK neurons. We measured the activity of SELKs while artificially activating either GRN population (Fig. 1c, f). We observed a sustained elevation of calcium levels in SELKs upon stimulation of bitter GRNs by light (Fig. 1d, e). Similarly, we observed an increase in calcium levels in SELKs upon activation of sweet GRNs by light (Fig. 1g), albeit to a smaller degree than when the bitter GRNs were activated (Fig. 1h). We did not observe such an increase in calcium levels in control animals not fed with all-trans retinal (ATR), the necessary co-factor for CsChrimson (Supplementary Fig. 3a, b). Next, we sought to measure the SELK activity in response to the introduction of either bitter (Fig. 1i) or sweet (Fig. 1l) tastants to the proboscis. In fed animals, we observed an increase in GCaMP fluorescence levels in SELKs upon bitter stimulation of the proboscis (Fig. 1j), while sweet stimulation had no significant effect (Fig. 1m). Since starvation increases the sensitivity of sweet GRNs to sweet substances<sup>10,11,50,51</sup>, we sought to examine whether it would also lead to an increase in SELK response. Remarkably, we observed that in starved animals, both bitter and sweet stimulation led to significant increases in GCaMP fluorescence levels in SELKs (Fig. 1k, n). These observations indicate that both bitter and sweet GRNs are presynaptic to SELKs and that the activation of either GRN population can lead to the activation of SELKs, depending on the feeding state of the animal.

Our observation that SELKs are both anatomically and functionally connected to taste modalities that elicit opposing behavioral outcomes poses an intriguing question: could SELKs be regulating both opposing behavioral outcomes, and, if yes, how? To address this question, we characterized the contributions of SELKs to feeding behaviors, starting with their involvement in bitter taste avoidance.

To this end, we sought to inhibit the SELKs and assess the behavioral consequences. Since the other LK neurons are implicated in various aspects of feeding behavior<sup>36–38,52</sup>, we generated two driver lines, SELK1 and SELK2, with selective expression in SELKs and a few other neurons (Supplementary Notes, Supplementary Fig. 4).

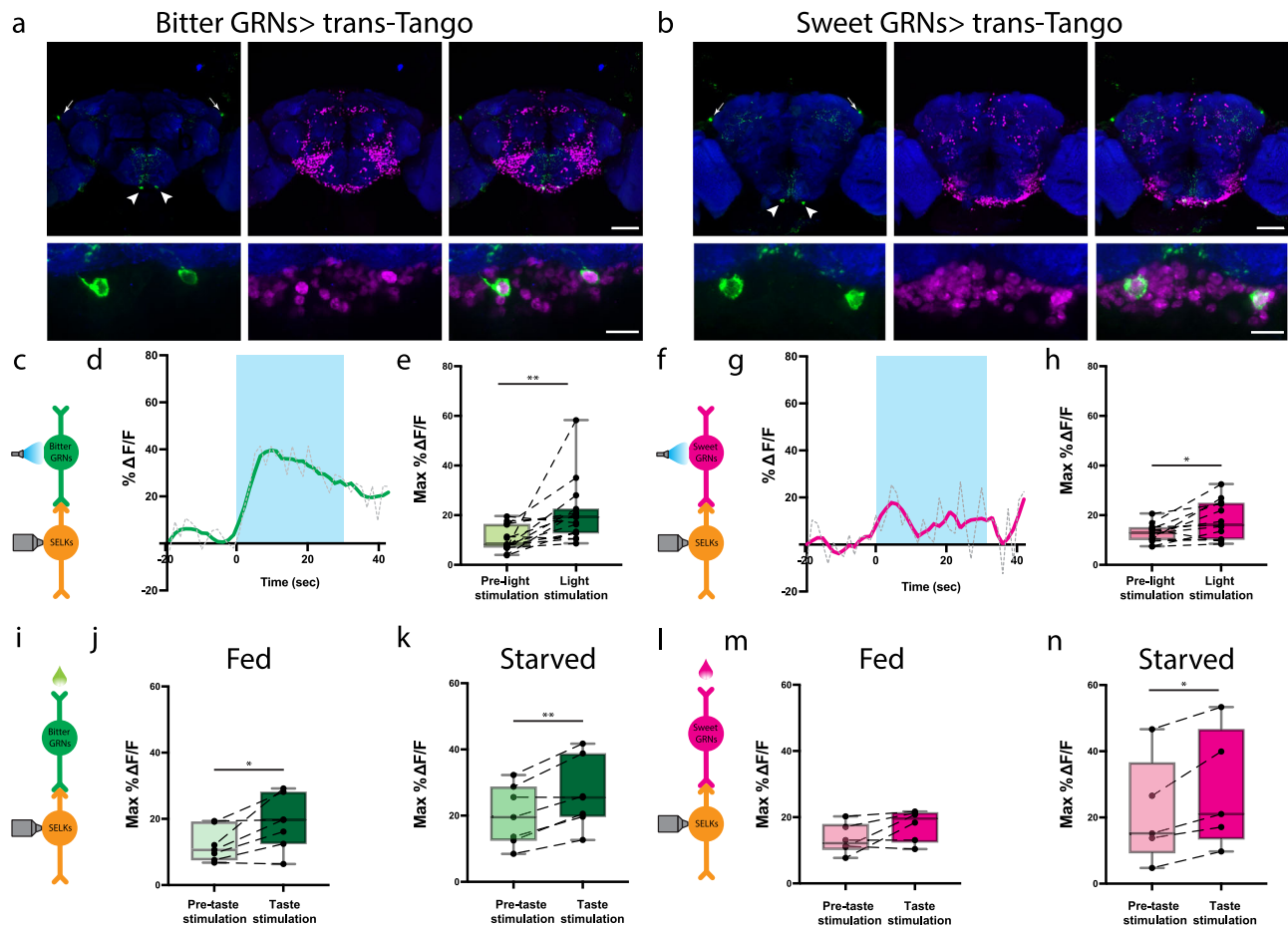


**Fig. 1 | SELKs are anatomically and functionally connected to both bitter and sweet GRNs.** **a, b** Staining the central brain with an antibody against LK (green) labels a pair of neurons in the lateral horn (LHLKs, arrow) and a pair in the ventral SEZ (SELKs, arrowhead). The nuclei of the postsynaptic partners of bitter-GRNs (**a**) and sweet-GRNs (**b**) as revealed by *trans*-Tango, are shown in magenta. The merge images in the right panels reveal colocalization of the LK immunostaining with the postsynaptic *trans*-Tango signal in SELKs but not in LHLKs. Zoomed-in images of the SEZ are shown at the bottom panels of (**a, b**). Scale bars: 50  $\mu$ m for top and 10  $\mu$ m for bottom panels. Neuropil staining is shown in blue. Optogenetic activation of bitter GRNs (**c–e**), or sweet GRNs (**f–h**) in conjunction with calcium imaging of SELKs. Schematics of the experiments in which bitter GRNs (**c**), or sweet GRNs (**f**) are optogenetically activated, and activity of SELKs is monitored by *in vivo* calcium imaging. Individual traces from imaging sessions of SELKs while either bitter GRNs (**d**), or sweet GRNs (**g**) are optogenetically activated ( $n = 16$  and  $13$ , respectively). The blue-shaded area indicates the time frame in which the light is on. Dotted lines

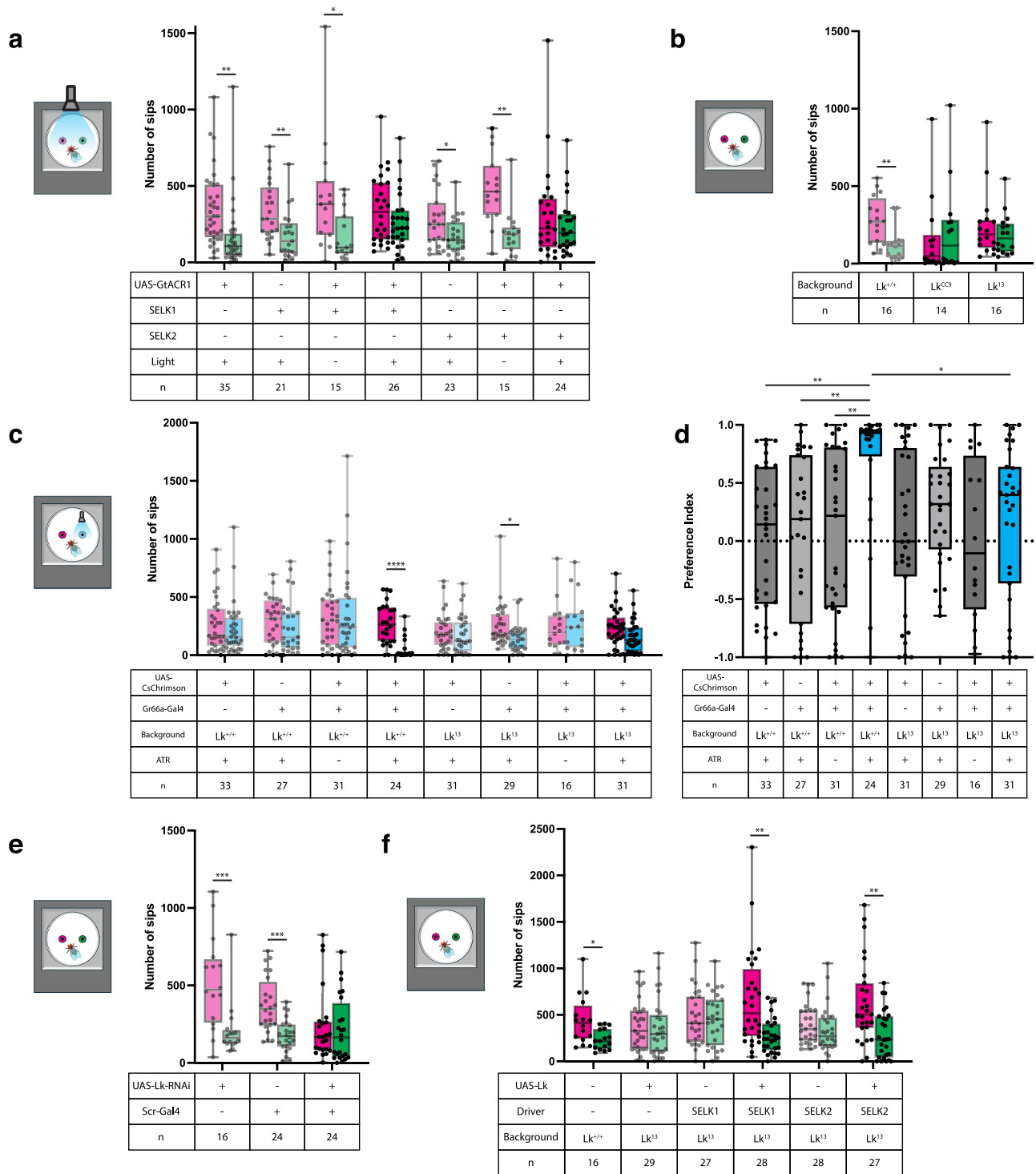
indicate the actual data points, and the solid lines indicate the smoothed curve. **e, h** Note the significant increases in the maximum fluorescence levels in SELKs during light stimulation of both bitter GRNs ( $n = 15$ , biological replicates, two-tailed  $P = 0.0077$ , **e**) and sweet GRNs ( $n = 13$ , biological replicates, two-tailed  $P = 0.0142$ , **h**) compared to the baseline before light stimulation. Paired t-test. **i–n** Calcium imaging of SELKs during administration of either 10 mM lobeline (a bitter compound) (**i–k**), or 1 M sucrose (a sweet compound) (**l–n**), to the fly's proboscis. In fed flies, SELKs exhibit elevated  $Ca^{++}$  levels in response to bitter ( $n = 7$ , biological replicates, two-tailed  $P = 0.0255$ , **j**) but not to sweet tastants ( $n = 6$ , biological replicates, two-tailed  $P = 0.0924$ , **m**). By contrast, in starved flies, there is a significant increase in the GCaMP signal upon delivery of bitter ( $n = 7$ , biological replicates, two-tailed  $P = 0.0031$ , **k**), or sweet ( $n = 5$ , biological replicates, two-tailed  $P = 0.0167$ , **n**) tastants. Paired t-test.  $P$ -values for all statistical tests:  $^* \leq 0.05$  and  $^{**} \leq 0.01$ . Boxplots indicate median (middle line), 25th and 75th percentile (box), bars represent maximum and minimum. Source data are provided as a Source data file.

Importantly, SELKs are the only shared neurons between these two split Gal4 drivers. Therefore, we used both drivers in all subsequent experiments to examine the specific roles of SELKs in feeding behavior.

### SELKs mediate bitter avoidance in an LK-dependent manner

To examine defects in bitter avoidance associated with SELKs, we used a modified optoPAD assay<sup>53</sup> while optogenetically inhibiting SELKs via GtACRI<sup>54</sup>. In this paradigm, the flies could choose between two equally sweet solutions, one of which was mixed with a low concentration of lobeline, a bitter compound (bittersweet), and the numbers of sips were scored. Control flies carrying either the driver or the effector alone, as well as controls carrying both alleles but not exposed to light, exhibited bitter avoidance, taking significantly fewer sips from the bittersweet solution. By contrast, experimental flies in which SELKs were inhibited took similar numbers of sips from both solutions (Fig. 2a). These results indicate that SELK activity is necessary for bitter avoidance.

We next sought to address the involvement of LK in bitter avoidance. To this end, we tested both a published Lk mutant (Lk<sup>CC9</sup>)<sup>26</sup> and a new null mutant, termed Lk<sup>13</sup>, which we generated using CRISPR-Cas9-mediated genome editing (see Supplementary Notes, Supplementary Fig. 5a, b). To eliminate the confounding effects of the feeding deficits exhibited by Lk<sup>CC9</sup>, we chose 1 M sucrose, a concentration at which Lk mutants exhibit comparable amount of feeding to controls (see Supplementary Notes and Supplementary Fig. 5c). We subjected the flies to a two-choice feeding assay on flyPAD, where they could choose between sweet and bittersweet, as described above. While control flies fed significantly less from the bittersweet food than from the sweet option, flies from both mutant lines took similar numbers of sips from either food option, indicating a deficiency in bitter avoidance (Fig. 2b). Remarkably, total feeding (i.e., number of sips taken from sweet + number of sips taken from bittersweet mixture) was not significantly different between the control group and either of the mutant



groups (Supplementary Fig. 5d). Next, we asked whether this effect can be generalized to other bitter compounds. To this end, we replaced lobeline with either quinine or denatonium and subjected the control and mutant flies to two-choice feeding assays. While controls effectively avoided the bittersweet mixture, flies from both Lk mutant groups took similar numbers of sips from either food option, further affirming the deficiencies in bitter avoidance in the absence of LK signaling (Supplementary Fig. 5e, f). We confirmed these results in existing<sup>26</sup> and newly generated mutants of the LK receptor (see Supplementary Notes and Supplementary Fig. 6a, b). We observed that total feeding was also reduced in the receptor mutants (Supplementary Fig. 6c), an effect we speculate to stem from LK-independent

activity of the receptor. Together, these results indicate that LK signaling is necessary for proper bitter avoidance.

To further confirm that Lk mutants are deficient in bitter avoidance, we tested whether optogenetic activation of bitter GRNs would suppress feeding in Lk mutants. To this end, we expressed CsChrimson in bitter GRNs in either Lk<sup>13</sup> mutant or control Lk<sup>+/+</sup> background. We presented flies in an optoPAD assay with two identical food options of 1 M sucrose and paired one with a 2-s light pulse to activate the bitter GRNs. While Lk<sup>+/+</sup> animals strongly avoided the option paired with activation of bitter GRNs (preference index (PI), mean = 0.68, median = 0.93), Lk<sup>13</sup> mutants exhibited no such avoidance (PI mean = 0.17, median = 0.40) (Fig. 2c, d). We observed similar results comparing

**Fig. 2 | LK expression in SELKs is necessary and sufficient for bitter avoidance.**

Two-choice feeding assays in different conditions. In each panel, the schematic presents the experimental paradigm, while the alleles expressed by each group of flies, the presence of ATR in the food, light condition (where applicable), and the number of animals in each group are indicated in the tables below the plots. Genetic controls are presented in lighter shades. **a** A two-choice feeding assay with flies in which GtACR1 is expressed in SELKs using the SELK1 or SELK2 drivers. The total numbers of sips taken from either sweet (magenta) or bittersweet (green) are plotted. The light is kept on throughout the experiment for continuous optogenetic inhibition. Paired t-test. Two-tailed *P* values are 0.003, 0.009, 0.038, 0.207, 0.023, 0.001, 0.421, respectively. **b** Lk mutants ( $Lk^{13}$ ) along with the  $w^{1118}$  control group ( $Lk^{+/+}$ ) are tested on a two-choice feeding assay. The total numbers of sips taken from either sweet (magenta) or bittersweet (green) are plotted. Paired t-test. Two-tailed *P* values are 0.006, 0.651, and 0.439, respectively. **c** An optoPAD two-choice assay with flies expressing CsChrimson in bitter GRNs either in  $w^{1118}$  control background ( $Lk^{+/+}$ ) or  $Lk^{13}$  mutant background. The total number of sips taken from either sweet (magenta) or sweet paired with a pulse of light (cyan) are plotted.

Paired t-test. Two-tailed *P* values are 0.522, 0.563, 0.961, <0.0001, 0.581, 0.012, 0.727, and 0.093, respectively. **d** Preference indices of the control and experimental groups from the same optoPAD two-choice assay presented in (c). Experimental groups are indicated in cyan, while the controls are presented in gray. The dashed line indicates a PI of 0, which means no preference for either food option. One-way ANOVA. Adjusted *P* values are 0.001, 0.003, 0.002, and 0.015, respectively. **e** A two-choice feeding assay with flies in which LK expression is knocked down using the Scr driver and LK RNAi. Paired t-test. Two-tailed *P* values are 0.0009, 0.0001, and 0.739, respectively. **f** Rescue experiments in which the Lk expression is restored only in SELKs using SELK1 or SELK2 drivers in the  $Lk^{13}$  mutant background. The flies are subjected to the two-choice feeding assay, and the total numbers of sips taken either from sweet (magenta) or bittersweet (green) are plotted. Paired t-test. Two-tailed *P* values are 0.019, 0.652, 0.781, 0.001, 0.356, and 0.005, respectively. Boxplots indicate median (middle line), 25th and 75th percentile (box), bars represent maximum and minimum. For all panels, *n* indicates biological replicates. Source data are provided as a Source data file.

animals in the  $Lk^{+/+}$  control and  $Lk^{CC9}$  mutant backgrounds: while activation of bitter neurons led to a strong food aversion in the control background (PI mean = 0.85, median = 0.91), this avoidance was abolished in  $Lk^{CC9}$  mutants (PI mean = 0.1861, median = -0.083, Supplementary Fig. 5g, h). These observations further demonstrate the necessity of LK for bitter avoidance.

We next examined whether LK expression in SELKs is required for bitter avoidance. To selectively manipulate SELKs, we searched for driver lines that label SELKs but not the other LK neurons. We identified a candidate, the Homeobox gene *sex combs reduced* (*Scr*), since the *Scr* driver labels neurons in the ventral SEZ<sup>55</sup>. Further, the single-cell transcriptomic analysis of the fly brain<sup>56</sup> shows an overlap between *Scr* and a small subset of LK-producing cells (Supplementary Fig. 7a), likely the SELKs. Indeed, when we expressed green fluorescent protein (GFP) under the control of the *Scr* driver, we observed that it labels both SELKs and no other LK neuron (Supplementary Fig. 7b–d). We then used the *Scr* driver to selectively knockdown Lk expression<sup>28</sup> in SELKs using RNA interference (RNAi). First, we confirmed the efficacy of the knockdown approach by LK immunostaining. We drove expression of the Lk RNAi with the *Scr* driver and observed a dramatic reduction in the LK signal in SELKs (Supplementary Fig. 7e). When tested on the two-choice feeding assay, flies expressing the Lk RNAi in SELKs did not exhibit bitter avoidance (Fig. 2e). Together, these results indicate that LK expression in SELKs is necessary for bitter avoidance.

Next, we tested whether bitter avoidance could be restored by selectively reintroducing LK to SELKs in the Lk mutant background using our SELK drivers. First, we used immunohistochemistry to validate the selective expression of LK in SELKs. We used the SELK1 or SELK2 drivers to express the Lk transgene in  $Lk^{13}$  mutant background and stained for LK. We observed LK staining only in SELKs and not in the other LK neurons (Supplementary Fig. 8a, b). Notably, with the SELK2 driver, we observed an ectopic pair of LK<sup>+</sup> neurons in the *pars intercerebralis* (Supplementary Fig. 8b). When subjected to the bitter avoidance paradigm,  $Lk^{13}$  mutant flies carrying either the driver or effector alleles alone exhibited no significant difference in feeding between the two food options. Conversely, flies in which LK expression is restored in SELKs using either driver exhibited bitter avoidance to a similar degree as  $Lk^{+/+}$  flies (Fig. 2f). These results demonstrate that the expression of LK in SELKs is sufficient for proper bitter avoidance.

**Activation of SELKs induces food aversion in an LK-dependent manner**

Since LK expression in SELKs is necessary for bitter avoidance, we wished to examine whether activation of SELKs is sufficient to suppress feeding. First, we examined the effects of activation of all LK neurons on feeding. To this end, we expressed CsChrimson in all LK neurons and subjected the flies to a two-choice optoPAD paradigm where the

flies are presented with two identical sweet food options and feeding on one of the options triggers a pulse of light. Activation of all LK neurons resulted in a strong aversion (Fig. 3a), with a much higher preference for the sweet-only option (PI mean = 0.59, median = 0.85) (Fig. 3b). Remarkably, this aversion requires LK since activation of all LK neurons in the  $Lk^{13}$  mutants did not result in aversion (Fig. 3a). The Lk-dependence of the aversion is also manifested as a lower preference for the sweet-only option in Lk mutants (PI mean = 0.090, median = 0.29) than in flies with intact LK expression (Fig. 3b). We next corroborated these results in the other Lk mutant background,  $Lk^{CC9}$ . Importantly, this mutant line was generated through a Gal4 insertion into the 5'-end of the coding sequence of Lk<sup>26</sup>, and it expresses in a few non-LK neurons (Supplementary Fig. 9a). Additionally, we failed to generate a line with CsChrimson in the  $Lk^{CC9}$  mutant background. To circumvent these shortcomings, we generated a transgenic fly line expressing LexA under the Lk promoter. This line recapitulated the expression of the Lk-Gal4 line<sup>39</sup> with expression in a few additional neurons in the optic lobes and the anterior ventrolateral protocerebrum (Supplementary Fig. 9b). Activation of LK neurons using the Lk-LexA driver leads to robust food aversion (Supplementary Fig. 9c) and a high preference for the sweet only option (PI mean = 0.64, median = 0.85) (Supplementary Fig. 9d). By contrast, activation of the LK neurons using the same driver in the  $Lk^{CC9}$  mutant background did not result in an aversion to the food paired with light (PI mean = 0.20, median = 0.24) (Supplementary Fig. 9d). Thus, the experiments with the  $Lk^{CC9}$  line corroborated the results obtained in the  $Lk^{13}$  mutant background. Taken together, our results with both mutants reveal that LK is necessary for the effects of LK neurons on food aversion. To assess the role of SELKs in the food aversion phenotype, we used the two SELK drivers to express CsChrimson and subjected the flies to the same experimental paradigm. We observed a similar food aversion phenotype upon activation of SELKs (Fig. 3c). These observations indicate that the activation of SELKs is sufficient to drive food aversion.

We next wished to examine whether the optogenetic activation of SELKs indeed leads to secretion of the neuropeptide. To test this, we optogenetically activated SELKs at the same light intensity used in the behavioral experiments ( $15.46 \mu\text{W}\cdot\text{mm}^{-2}$ ), dissected the flies, and stained the brains with antibodies against LK. We compared the numbers of puncta in the neurites of SELKs in flies subjected to light and controls kept in the dark. We observed significantly fewer puncta when SELKs are optogenetically activated, indicating LK release (Fig. 3d). Next, we examined the release of LK from SELKs upon optogenetic activation of bitter GRNs. Strikingly, we observed a significant reduction in the number of puncta in SELKs upon light activation of bitter GRNs compared to flies kept in the dark (Fig. 3e). These results demonstrate that SELKs release LK upon activation of bitter GRNs and further confirm the functional connection between bitter

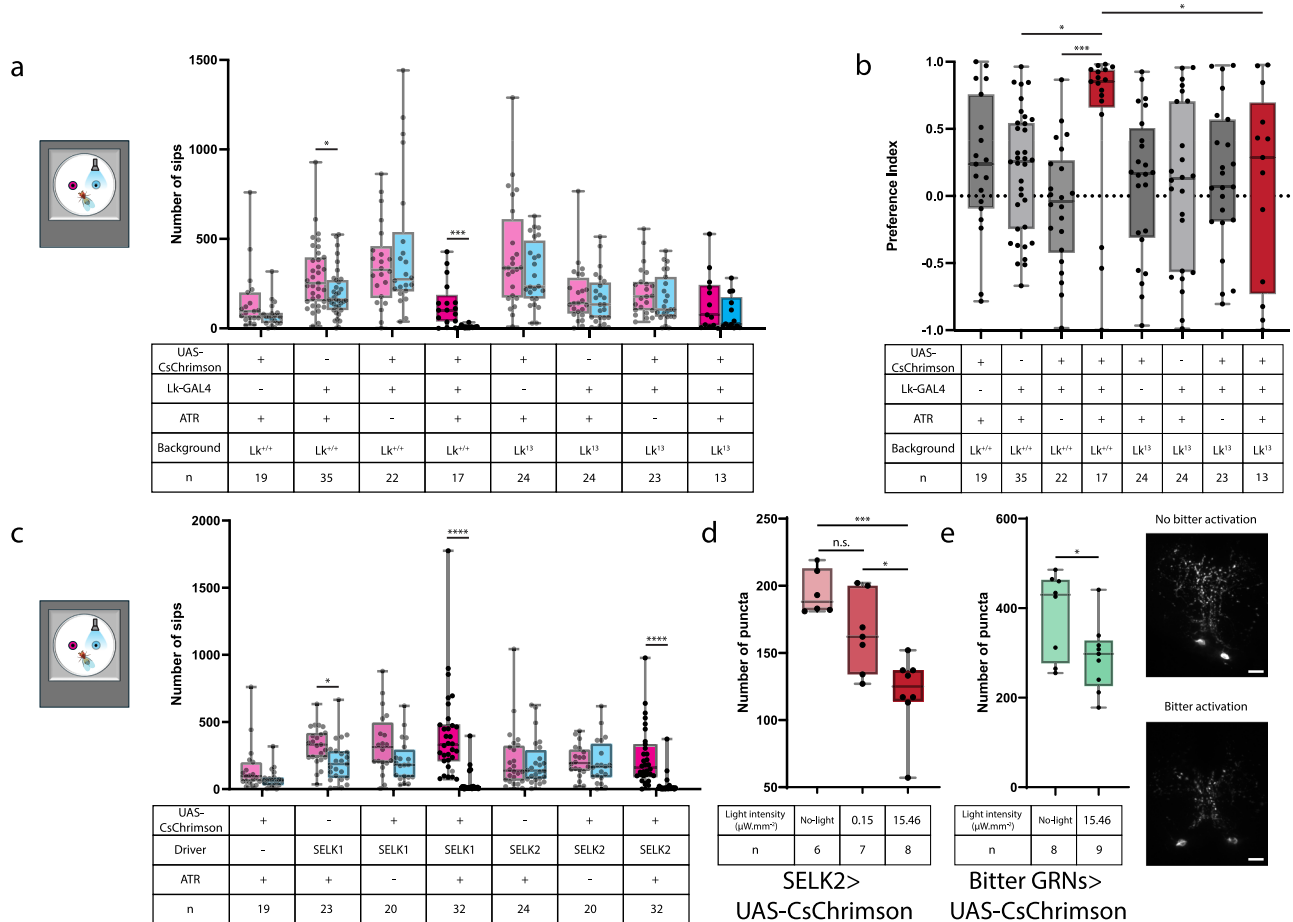


**Fig. 3 | Activation of SELKs induces food aversion in an LK-dependent manner.**

**a–c** Two-choice optoPAD assays. In each panel, the schematic presents the experimental paradigm, while the alleles expressed by each group of flies, the presence of ATR in the food, and the number of animals in each group are indicated in the tables below the plots. Genetic controls are presented in lighter shades. **a** The flies express CsChrimson in LK neurons in either the  $w^{1118}$  control background (Lk<sup>+/+</sup>) or the Lk<sup>13</sup> mutant background. The total number of sips taken from either sweet (magenta) or sweet paired with a pulse of light (cyan) are plotted. Paired t-test. Two-tailed *P* values are 0.130, 0.021, 0.347, 0.0008, 0.225, 0.635, 0.403, and 0.176, respectively. **b** Preference indices of the control and experimental groups from the same experiment presented in **(a)**. Experimental groups are indicated in red, while the controls are presented in gray. The dashed line indicates a PI of 0, meaning no

preference for either food option. One-way ANOVA. Adjusted *P* values are 0.139, 0.033, 0.0008, and 0.039, respectively. **c** The flies express CsChrimson in SELKs via the SELK1 or SELK2 drivers. Paired t-test. Two-tailed *P* values are 0.130, 0.0225, 0.080, <0.0001, 0.766, 0.859, and <0.0001, respectively. **d, e** Secretion of LK from SELKs. The number of SELK puncta following optogenetic activation of SELKs using the SELK2 driver (one-way ANOVA, adjusted *P* values are 0.117 for no light vs. 0.15  $\mu\text{W mm}^{-2}$ , 0.0001 for no light vs. 15.46  $\mu\text{W mm}^{-2}$ , and 0.012 for 0.15  $\mu\text{W mm}^{-2}$  vs. 15.46  $\mu\text{W mm}^{-2}$ , **d** or the bitter GRNs (unpaired t-test, the two-tailed *P* value is 0.034, **e**) at different light intensities. Representative images are shown. Scale bars: 10  $\mu\text{m}$ . Boxplots indicate median (middle line), 25th and 75th percentile (box), bars represent maximum and minimum. For all panels, *n* indicates biological replicates. Source data are provided as a Source data file.

GRNs and SELKs. Together, these observations indicate that SELKs release LK in response to aversive gustatory stimuli and that LK release is necessary to elicit food rejection.

### SELKs promote feeding via acetylcholine

Given that SELKs are also postsynaptic to sweet-sensing Gr64f<sup>+</sup> neurons, we wished to examine whether they have an additional, opposing role in promoting food intake. To test this, we drove GtACR1 by SELK1 or SELK2 to selectively inhibit SELKs. In this paradigm, we provided the same food in both wells of the optoPAD and kept the light on throughout the experiment to constantly inhibit the neurons. We used 100 mM sucrose here rather than the 1 M used in the two-choice experiments to prevent the animals from reaching satiety and keep the responses to food within a dynamic range (Supplementary Fig. 5c). We observed that the inhibition of SELKs resulted in fewer sips compared to controls (Fig. 4a). These results were corroborated by expression of GtACR1 in all LK neurons using the Lk-Gal4 driver that also resulted in a decrease in the number of sips taken (Fig. 4a). Since SELKs are the only common neurons labeled by these three drivers (SELK1, SELK2 and Lk-

Gal4), we concluded that inhibition of SELKs during feeding leads to a decrease in food intake, suggesting an additional role of SELKs in promoting feeding.

In view of these results and our earlier observation that Lk mutants exhibit a decrease in food intake (Supplementary Fig. 5c), we wished to examine whether the effect of SELKs on food intake requires Lk expression. To test this, we knocked down Lk expression in SELKs using the Scr driver to express RNAi for Lk and scored the number of sips taken from 100 mM sucrose. To our surprise, rather than a decrease in the number of sips, knocking down Lk in SELKs resulted in a slight increase (Supplementary Fig. 10a). To further assess the role of Lk expression in SELKs, we attempted to rescue the decrease in food intake exhibited by Lk mutants. To this end, we restored the expression of Lk in SELKs in the Lk<sup>13</sup> mutant background. However, this manipulation did not rescue the decreased food intake either (Supplementary Fig. 10b). We next wished to examine whether activation of sweet GRNs induces LK release from SELKs. To achieve this, we optogenetically activated sweet GRNs and scored the number of LK puncta in SELKs. Unlike the activation of bitter GRNs, the activation of sweet

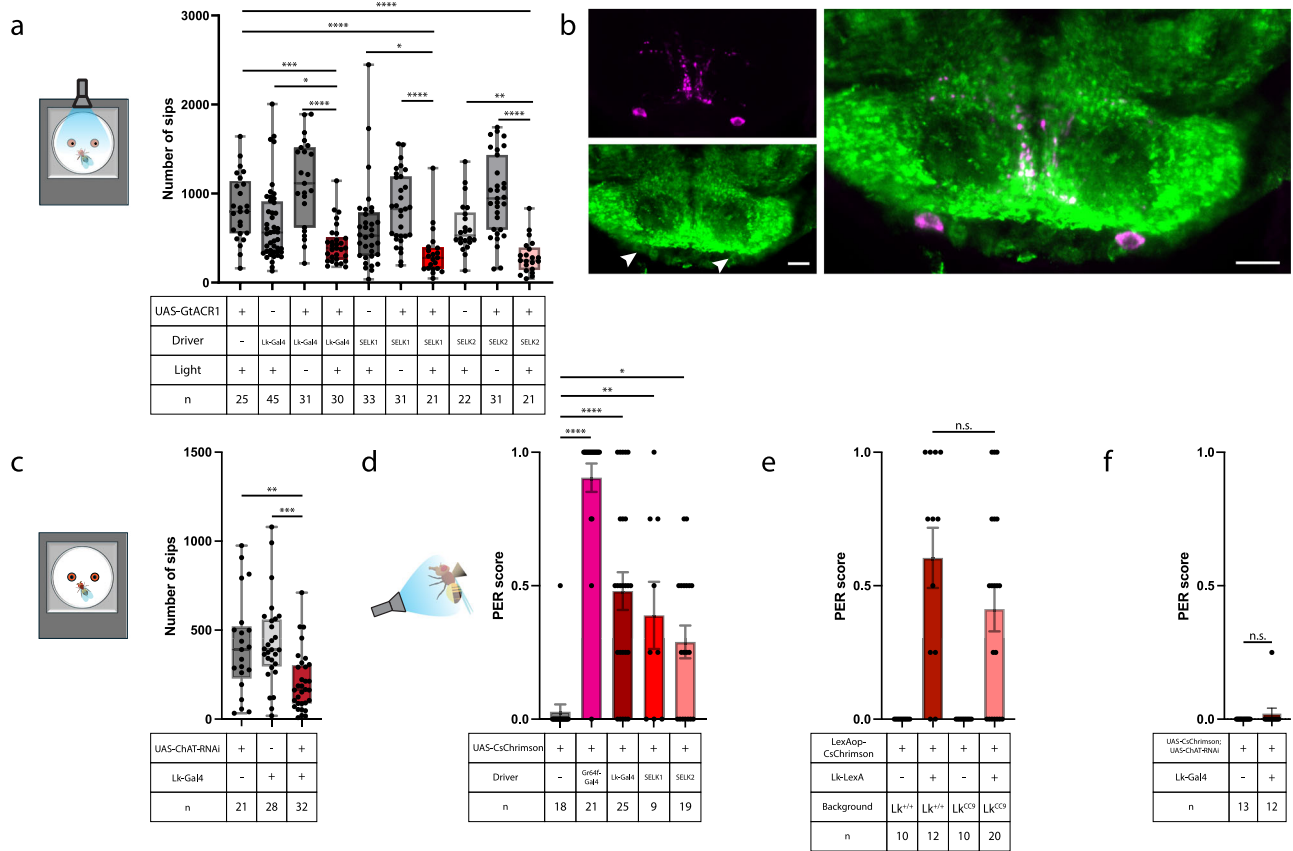


**Fig. 4 | SELKs promote feeding via acetylcholine. a** The effects of SELK inhibition on feeding. A flyPAD feeding assay with flies in which GtACR1 expression is driven by Lk-Gal4 (dark red), SELK1 (red) or SELK2 (light red). Genetic controls bearing either allele alone, or controls bearing both alleles but not exposed to light, are shown in shades of gray. The light is kept on throughout the experiment for continuous optogenetic inhibition. One-way ANOVA. Adjusted *P* values are 0.0004 for Lk > GtAcR1 vs. UAS-GtAcR1, 0.038 for Lk > GtAcR1 vs. Lk-Gal4, <0.0001 for Lk > GtAcR1 vs. Lk-Gal4 > GtAcR1 no light, <0.0001 for SELK1 > GtAcR vs. UAS-GtAcR1, 0.036 for SELK1 > GtAcR vs. SELK1, <0.0001 for SELK1 > GtAcR vs. SELK1 > GtAcR1 no light, <0.0001 for SELK2 > GtAcR1 vs. UAS-GtAcR1, 0.008 for SELK2 > GtAcR1 vs. SELK2, and <0.0001 for SELK2 > GtAcR1 vs. SELK2 > GtAcR1 no light. **b** SELKs revealed by staining with an antibody against LK (magenta) are colabeled with an antibody against ChAT (green). Arrowheads mark the SELKs among the ChAT<sup>+</sup> neurons. Scale bar: 10  $\mu$ m. **c** In a flyPAD feeding assay with flies in which ChAT expression is knocked down in LK neurons (red), the total numbers of sips are plotted. Genetic controls are indicated in shades of gray. One-way ANOVA. Adjusted *P* values are 0.004 and 0.0007, respectively. **d–f** Quantification of PER upon

light stimulation in optogenetic experiments. **d** Driving CsChrimson expression in sweet GRNs (magenta) and in neurons labeled by Lk-Gal4 (dark red), SELK1 (red) and SELK2 (light red). One-way ANOVA. Adjusted *P* values are <0.0001 for UAS-Chrimson vs. Gr64f > Chrimson, 0.008 for UAS-Chrimson vs. SELK1 > Chrimson, 0.020 for UAS-Chrimson vs. SELK2 > Chrimson, and <0.0001 for UAS-Chrimson vs. Lk > Chrimson. **e** Driving CsChrimson expression in Lk neurons via Lk-LexA either in the *w<sup>1118</sup>* background (Lk<sup>+/+</sup>) (dark red) or in the Lk<sup>CC9</sup> mutant background (light red). Unpaired t-test with Welch's correction, the two-tailed *P* value is 0.186. **f** Optogenetic activation of Lk neurons while the expression of ChAT is down-regulated. Unpaired t-test with Welch's correction. The two-tailed *P* value is 0.3388. Error bars indicate the standard error of the mean. In each panel of the behavioral experiments, the schematic presents the experimental paradigm, while the alleles expressed by each group of flies and the numbers of animals in each group are indicated in the tables below the plots. Boxplots indicate median (middle line), 25th and 75th percentile (box), bars represent maximum and minimum. For all panels, *n* indicates biological replicates. Source data are provided as a Source data file.

GRNs did not result in a decrease in the number of LK puncta in SELKs (Supplementary Fig. 10c), indicating that sweet GRNs do not induce LK secretion from SELKs. We concluded that the effect of SELKs in promoting feeding is not mediated by LK and hypothesized that SELKs regulate food intake using another neurotransmitter.

To identify the putative neurotransmitter produced by SELKs, we decided to mine the single-cell transcriptomic atlas of the fly brain<sup>56</sup>. We examined every cell with high levels of Lk reads and, through a process of elimination, identified the various LK neuron subtypes. We could reliably identify ALKs using the marker genes ion transport peptide, short neuropeptide F, tachykinin, and LKR, known to be expressed by this population<sup>25,41,57</sup> (Supplementary Fig. 7a). Similarly, we identified lateral horn LK neurons (LHLKs) by the expression of the transcription factor *apterous* (*AP*), known to be expressed only in LHLKs among LK neurons<sup>58</sup>. The three remaining LK neurons are all positive for *Scr*, the SEZ marker we used in our knockdown experiments. Notably, two of these are positive for choline acetyltransferase

(ChAT) transcripts, a marker for cholinergic neurons<sup>59</sup>. We, therefore, hypothesized that SELKs use ACh as the neurotransmitter that carries out the antagonistic functions to those mediated by the LK peptide. To examine whether SELKs are indeed cholinergic, we performed immunostaining experiments with antibodies against LK and ChAT. We observed colocalization of the two signals in SELKs (Fig. 4B), but not in LHLKs (Supplementary Fig. 10d) or ABLKs (Supplementary Fig. 10e). To further confirm that SELKs are cholinergic, we expressed GFP in all cholinergic neurons and stained the brains with the antibody against LK. We observed colocalization of GFP and LK staining only in SELKs (Supplementary Fig. 10F, F'). Notably, the observation that SELKs are cholinergic is also in line with the EM data predictions<sup>45</sup>. Taken together, these findings reveal that SELKs produce both LK and ACh and are the only cholinergic LK neurons.

To assess the role of ACh production by SELKs in regulating food intake, we knocked down ACh production by expressing an RNAi targeting the ChAT transcript<sup>60</sup> using the Lk driver. Since SELKs are the

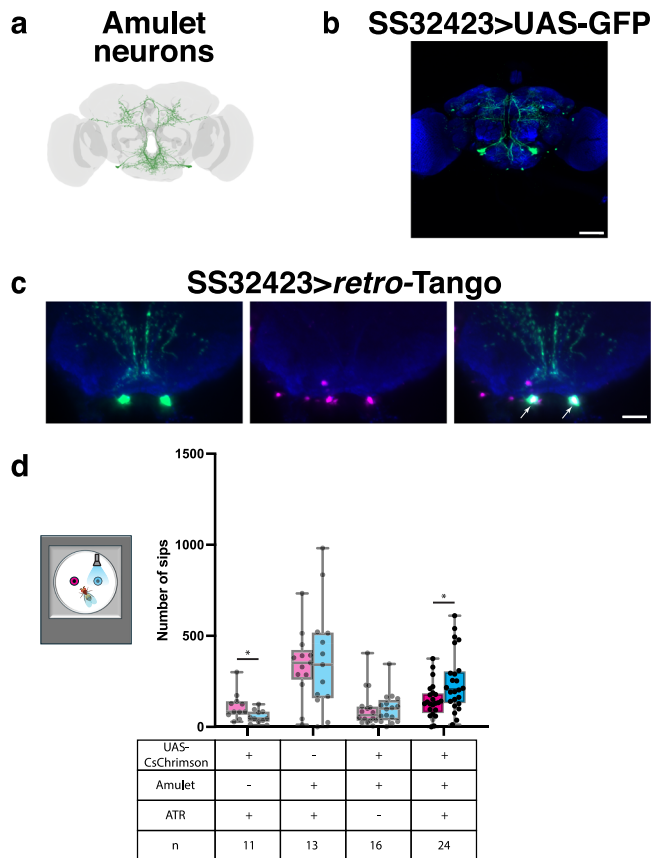


**Fig. 5 | Amulet neurons are postsynaptic to SELKs, and their activation promotes feeding.** **a** Rendering of the Amulet neurons from the EM reconstruction of a fly brain. Brain mesh is previously described<sup>46</sup> and is under CC BY-NC 4.0 license (<https://creativecommons.org/licenses/by-nc/4.0/>). **b** The split Gal4 driver SS32423 provides genetic access to the Amulet neurons. Flies bearing the SS32423 driver and UAS-GFP are stained with an antibody against GFP (green). Neuropil is shown in blue. Scale bar: 50  $\mu$ m. **c** The presynaptic inputs into the Amulet neurons are revealed by *retro-Tango*. The SS32423 driver drives *retro-Tango* from the Amulet neurons, revealing their presynaptic partners (magenta). SELKs are marked by staining with an antibody against LK (green). The merge image shows that SELKs (arrows) are costained with the presynaptic marker. Neuropil is shown in blue. Scale bar: 10  $\mu$ m. **d** In a two-choice optoPAD assay, the flies express CsChrimson in Amulet neurons using the SS32423 driver. The total number of sips taken from either sweet (magenta) or sweet paired with a pulse of light (cyan) are plotted. Genetic controls are presented in lighter shades. Paired t-test. Two-tailed *P* values are 0.030, 0.798, 0.928, and 0.018, respectively. Boxplots indicate median (middle line), 25th and 75th percentile (box), bars represent maximum and minimum. For all panels, *n* indicates biological replicates. Source data are provided as a Source data file.

only cholinergic LK neurons, this manipulation should only affect ACh production by SELKs. In the no-choice paradigm where flies are presented with 100 mM sucrose in both wells, knocking down ChAT in SELKs resulted in a decrease in the number of sips compared to controls (Fig. 4c). Notably, down-regulation of ACh production in SELKs did not affect the bitter avoidance behavior (Supplementary Fig. 10g). These findings provide further evidence that SELKs modulate food intake through ACh.

To further determine how the cholinergic output from SELKs affects food intake, we sought to examine if SELK activation would influence the proboscis extension response (PER), a feeding behavior exhibited towards appetitive tastants<sup>61</sup>. As a positive control, we optogenetically activated the sweet-sensing Gr64f<sup>+</sup> GRNs<sup>14</sup>. Activation of these neurons was sufficient to drive all motor sub-programs of PER: rostrum lifting, as well as haustellum and labella extensions,

collectively constituting a full PER (Fig. 4d). Surprisingly, optogenetic activation of SELKs using SELK1, SELK2 or LK driver lines induced PER (Fig. 4d). However, the PER observed upon SELK activation was not as robust as the PER induced by activation of Gr64f<sup>+</sup> GRNs: it occurred at lower frequencies and the proboscis was not consistently fully extended. The partial extensions typically included rostrum lifting and labella extension, but not haustellum extension. These observations indicate that SELKs are involved in regulating PER, albeit to a lesser extent than the sweet-sensing GRNs.

We next wished to determine which of the neurotransmitters produced by SELKs affects PER: is it the neuropeptide LK or the fast-acting neurotransmitter ACh? To address this, we optogenetically activated LK neurons in Lk<sup>+/+</sup> background or Lk<sup>CC9</sup> mutant background. In these experiments, we used the Lk-LexA driver to express CsChrimson. We observed no significant difference in the PER elicited by the optogenetic activation of LK neurons in the Lk<sup>+/+</sup> background or Lk<sup>CC9</sup> mutant background (Fig. 4e). By contrast, optogenetic activation of the LK neurons while knocking down ChAT in SELKs did not induce PER (Fig. 4f). These results demonstrate that for SELK-induced PER, ACh production is necessary while LK secretion is dispensable.

### Amulet neurons are postsynaptic to SELKs and their activation promotes feeding

While neuropeptides can act extrasynaptically on distant targets, fast-acting neurotransmitters typically act synaptically. We, therefore, reasoned that the ACh-dependent, feeding-promoting effects of SELKs should be exerted synaptically. To identify the postsynaptic targets of SELKs and examine their roles in regulating food intake, we again turned to an EM reconstruction of a fly brain connectome<sup>43,46,47</sup>. Our analysis of the connectome revealed that downstream targets with which the SELKs make the most synaptic connections are either central or descending neurons. Most of these synaptic targets of SELKs are presynaptic to motor neurons that control the proboscis, and hence feeding (Supplementary Fig. 11a, b). Next, we activated SELKs in silico using a leaky integrate-and-fire computational model<sup>62</sup>. This analysis revealed that increasing the frequency of activation of SELKs elevated the activity of some descending neurons, motor neurons, and bilateral clusters of central neurons (body IDs 720575940635211768 and 720575940604470240) as the major postsynaptic partners of both SELKs (Fig. 5a and Supplementary Fig. 11c). These clusters had been identified as projection neurons from the SEZ and termed Amulet neurons<sup>12</sup>. Interestingly, each SELK neuron makes synaptic connections with the Amulet neurons on both hemispheres (ipsilaterally and contralaterally). We found that the Amulet neurons have extensive arborizations both in the SEZ and in the protocerebrum in both brain hemispheres (Fig. 5b). To confirm that the Amulet neurons are indeed postsynaptic to SELKs, we initiated *retro-Tango*<sup>63</sup> from the Amulet neurons and revealed that SELKs are presynaptic to them (Fig. 5c).

We next sought to examine the effects of the Amulet neurons on feeding. To this end, we expressed CsChrimson in these neurons and subjected the flies to the two-choice optoPAD paradigm. Strikingly, unlike the controls, the experimental flies exhibited a high preference for the food paired with light (Fig. 5d). Thus, activation of the Amulet neurons recapitulates the feeding-promoting effects of activation of SELKs. Together, these results suggest that the Amulet neurons are postsynaptic to SELKs and mediate the feeding-promoting effects of SELKs.

### SELKs elicit opposing feeding behaviors based on their level of activation

Collectively, the behavioral experiments indicate a dual role for SELKs in regulating feeding: they suppress it via LK release and induce it via ACh. Thus, SELKs act both as negative and positive regulators of feeding. What is the mechanism that enables SELKs to differentially

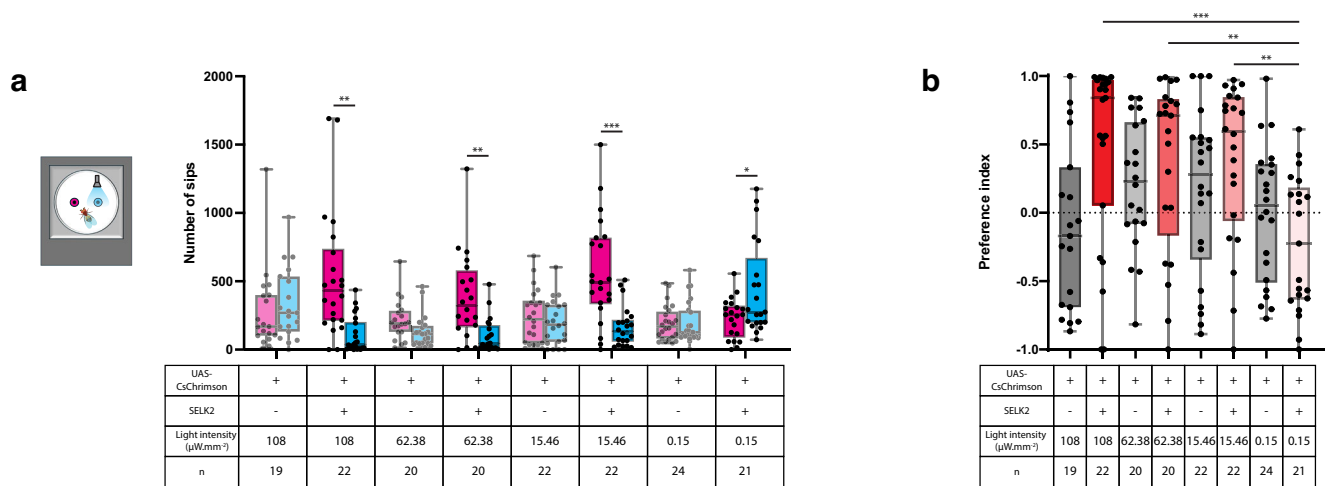


**Fig. 6 | SELKs differentially regulate feeding according to their level of activation. a** In a two-choice optoPAD assay, the flies express CsChrimson in SELK neurons using the SELK2 driver. The total number of sips taken from either sweet (magenta) or sweet paired with pulses of light at various intensities (cyan) are plotted. Genetic controls are presented in lighter shades. Paired t-test. Two-tailed  $P$  values are 0.605, 0.001, 0.060, 0.002, 0.417, 0.003, 0.981, and 0.029, respectively. **b** Preference indices of the control and experimental groups from the same experiment presented in (a). The increasing light intensities are presented by

increasing the darkness of the shades of red. Controls bearing only the CsChrimson allele are depicted in shades of gray. One-way ANOVA. Adjusted  $P$  values are 0.0005 for  $108 \mu\text{W}\cdot\text{mm}^{-2}$  vs.  $0.15 \mu\text{W}\cdot\text{mm}^{-2}$ , 0.005 for  $62.38 \mu\text{W}\cdot\text{mm}^{-2}$  vs.  $0.15 \mu\text{W}\cdot\text{mm}^{-2}$ , 0.003 for  $15.46 \mu\text{W}\cdot\text{mm}^{-2}$  vs.  $0.15 \mu\text{W}\cdot\text{mm}^{-2}$ . Boxplots indicate median (middle line), 25th and 75th percentile (box), bars represent maximum and minimum. For all panels,  $n$  indicates biological replicates. Source data are provided as a Source data file.

modulate feeding in opposing ways using two types of neurotransmitters?

Neuropeptides are released from dense core vesicles, which require high levels of activation for secretion<sup>64,65</sup>. By contrast, fast-acting neurotransmitters, like ACh, are released from synaptic vesicles that are smaller and closer to the synapse, and, therefore, more readily available for synaptic release<sup>66</sup>. We hypothesized that the different types of vesicles in which LK and ACh are stored enable their differential release in response to various degrees of neuronal activation. We, therefore, predicted that optogenetic activation of SELKs at different light intensities would elicit different feeding behaviors. To test this prediction, we subjected flies expressing CsChrimson in SELKs to the two-choice optoPAD paradigm, where they were given two identical food options, one of which paired with a light pulse. As controls, we used flies bearing only the CsChrimson transgene, but not the driver. We observed that at light intensities of 108, 62.38, and  $15.46 \mu\text{W}\cdot\text{mm}^{-2}$ , the experimental flies fed significantly less from the food paired with light (Fig. 6a), whereas controls did not exhibit any preference (Fig. 6b). Strikingly, when the food is paired with a low light intensity ( $0.15 \mu\text{W}\cdot\text{mm}^{-2}$ ), the experimental flies behaved in the opposite way and preferred the food paired with light, while the controls still exhibited no preference (Fig. 6b). Moreover, we observed no significant difference in the number of LK puncta in SELKs between flies exposed to this lower light intensity and flies kept in the dark (Fig. 3d). These results demonstrate that the activation of SELKs to various degrees can elicit opposing behaviors through differential neurotransmitter release. Low levels of activation lead to ACh release and induce feeding, while high levels of activation lead to LK release and food avoidance.

## Discussion

Feeding is a complex behavior controlled by an intricate network of regulatory systems. One class of modulators consists of an array of neuropeptides, many of which have been described<sup>21</sup>. We sought to identify the neuromodulatory systems that integrate taste information to elicit the appropriate feeding decisions by identifying neuropeptidergic neurons that receive direct input from GRNs. To achieve this, we implemented an anatomical screen using *trans*-Tango to identify

second-order neurons within the bitter and sweet gustatory circuits. This anatomical screen identified SELKs as postsynaptic to both bitter and sweet GRNs, as was recently reported<sup>67</sup>. While the proximity of the GRN projections and the neurites of SELKs had been previously noted<sup>39</sup>, our study provides evidence for direct anatomical and functional connectivity between GRNs and SELKs. Remarkably, SELKs receive input from gustatory modalities that typically elicit opposing feeding outcomes. This anatomical organization poses an interesting question as to how the same neurons can mediate opposing behavioral outcomes. Our experiments reveal that SELKs employ a dual transmission strategy in which a neuropeptide and a fast-acting neurotransmitter are used: LK release leads to food aversion, while ACh promotes food intake through induction of the PER motor program. This dual function underscores the complexity of SELK-mediated feeding regulation and highlights how a single neuron type can integrate conflicting sensory information to produce context-appropriate behaviors.

LK has been implicated in various aspects of feeding behavior, including the response to bitter tastants, regulation of meal size, and feeding decisions<sup>38,42,52</sup>. However, attribution of these functions to any of the four groups of LK neurons has been challenging, primarily due to the absence of specific drivers that selectively label each one. We overcome this problem by generating specific drivers that selectively label SELKs either through the intersection of split Gal4 drivers or by using a Gal4 driver that only labels SELKs among LK neurons. These driver lines have enabled us to dissect and characterize the specific functions of SELKs in taste processing and the control of feeding behavior.

Our study reveals that inhibition of SELKs leads to two opposing feeding impairments: a defect in food aversion, such as avoiding bitter tastants, and a reduction in overall food intake. We provide several lines of evidence that implicate LK release from SELKs in the negative regulation of feeding. First, the activation of SELKs suppresses food intake through LK release. Second, LK secretion from SELKs is necessary for proper bitter avoidance. Third, the deficiency in bitter avoidance exhibited by Lk mutants can be rescued by the selective expression of LK in SELKs. Interestingly, while the selective expression of LK in SELKs in the Lk mutant background restored the bitter

avoidance phenotype, the decreased food intake was not affected by this manipulation. Further, knocking down Lk in SELKs resulted in increased food intake. Remarkably, our study reveals that SELKs positively regulate feeding in an ACh-dependent manner, the opposite behavioral outcome to that of LK secretion. Our experiments indicate that SELKs use the fast-acting neurotransmitter ACh and that down-regulation of ACh production in SELKs mimics the decrease in food intake observed when SELKs are inhibited. Moreover, ACh production in SELKs is necessary for inducing PER by SELK activation. Thus, our study reveals that SELKs affect feeding through a dual transmission mechanism whereby LK release leads to food aversion, and ACh promotes feeding. Interestingly, selective control of different behaviors by a single neuron using distinct neurotransmitters was also observed in *Caenorhabditis elegans*<sup>30</sup>.

Our study suggests that SELKs exert their opposing effects on feeding through the differential release of neurotransmitters dependent on the activity level. Specifically, high level of activity in SELKs results in the release of LK from dense core vesicles and leads to the suppression of food intake. By contrast, low activation of SELKs leads to the release of synaptic vesicles that carry ACh, and consequently, to an increase in food intake. This interpretation of the results of the behavioral experiments is supported by our *in vivo* experiments in which we imaged calcium levels in SELKs in response to optogenetic activation of GRNs. These experiments revealed that SELK activation, measured as changes in calcium levels, is higher in response to the activation of bitter GRNs than to the activation of sweet GRNs. This observation is supported by calcium imaging experiments on SELKs upon delivery of bitter or sweet tastant. While the administration of bitter substances elicit responses in SELKs regardless of the food deprivation state, sweet substances elicit responses only when the animal is starved. We believe that the starvation-dependent response of SELKs to sweet substances occurs through the sensitization of sweet GRNs upon food deprivation<sup>10,11,50,51</sup>, since the basal activity of SELKs is unaffected by the food deprivation state<sup>25,28</sup>. Remarkably, a recent preprint revealed that in calcitonin gene-related peptide (CGRP) neurons in mice, dense core vesicles have a higher release threshold than that of synaptic vesicles<sup>32</sup>. Consequently, while aversive stimuli evoke high frequency responses and release of CGRP, appetitive stimuli induce low frequency responses and glutamate release to encode positive valence<sup>32</sup>. Thus, an analogous mechanism to what we observed in the fly SEZ is operative in the mouse hypothalamus.

In view of the complexity of feeding behavior, it is not entirely surprising that some aspects of it are counterintuitive. For example, while high levels of SELK activation might also lead to synaptic vesicle release, the net effect of this manipulation is food aversion. Thus, in this condition, the feeding-promoting effects of ACh release from SELKs might be overridden by LK release. In addition, when we activate the SELKs in the Lk mutant background with high light intensity, we do not observe the feeding-promoting effects of the ACh release. We speculate that the spillover ACh might inhibit the SELKs in an autocrine fashion. Alternatively, excess ACh might overwhelm the SELK circuit and mask its feeding-promoting effects. Interestingly, activation of SELKs at a light intensity of  $31.23 \mu\text{W}\cdot\text{mm}^{-2}$ —a light intensity higher than what we used in our two-choice optoPAD experiments ( $15.46 \mu\text{W}\cdot\text{mm}^{-2}$ ) where we observe feeding suppression—elicits PER. Thus, the motor program controlling PER is immune to the effects of LK, and the suppression of feeding by LK release bypasses PER.

We identified a pair of downstream synaptic partners of SELKs that had been previously described as projection neurons from the SEZ and named Amulet<sup>12</sup>. The connection between SELKs and the Amulet neurons is revealed both by analysis of a fly brain connectome and by *retro*-Tango experiments. Our experiments further reveal that activation of the Amulet neurons promotes feeding. Based on these findings, we propose that activation of SELKs by sweet GRNs promotes feeding via activation of the Amulet neurons, presumably through cholinergic

signaling. The Amulet neurons arborize extensively in both SEZ and protocerebrum, positioning them well to serve as a link between the gustatory system and higher-order brain areas that regulate feeding, such as the superior medial protocerebrum.

Our study also has implications for the model of gustatory information processing. Individual tastants have inherent valences: sweet tastants are appetitive and drive acceptance, while bitter compounds are aversive and elicit rejection. How the brain processes gustatory information has been a major topic of debate, with two main models describing taste coding. The labeled line model argues that the different taste modalities are processed through distinct, parallel, and non-overlapping channels. By contrast, the population coding model posits that taste coding is combinatorial, and inputs from different taste channels converge within the taste circuits. While labeled line processing is the prevailing model for taste coding in mammals<sup>68,69</sup>, how taste information is processed in insects is less clear. Some studies support the labeled line model<sup>5</sup>, while others support population coding<sup>18,34,70</sup>. Our study provides further support for the population coding model in *Drosophila*, as we uncover a node of integration between the sweet and bitter channels already at the level of second-order neurons in the gustatory circuits. Further, we reveal a mechanism by which these neurons can respond differentially to inputs from bitter and sweet GRNs that drive opposing behavioral outcomes.

Our study reveals that two types of GRNs that respond to bitter and sweet tastants and elicit opposing behavioral outcomes converge on a pair of neuropeptidergic neurons in the SEZ, the SELKs. The inherent challenge presented by this circuit organization is resolved by dual transmission of two different types of neurotransmitters, each affecting a different behavioral outcome. Activation of SELKs by bitter GRNs leads to the secretion of LK and results in food aversion. By contrast, activation of SELKs by sweet GRNs leads to the secretion of the fast-acting neurotransmitter ACh and results in the promotion of feeding. Further, the feeding-promoting effects of SELKs are mediated by a pair of SEZ projection neurons named Amulet that receive synaptic input from SELKs and project to the protocerebrum. The targets of SELKs that mediate food aversion via LK signaling are yet to be identified. Thus, our study provides an example for how the dual transmission of two different neurotransmitters enables the same neuron to modulate opposing behavioral outcomes.

## Methods

### Fly maintenance and husbandry

All flies used in this study were maintained at 25 °C, 70% humidity chambers with a 12-h light: 12-h dark cycle unless otherwise stated. All the animals were kept in standard cornmeal-agar-molasses media. The detailed genotypes of the animals used in this study can be found in Table 1. To minimize genetic variability, all lines used in behavioral experiments were backcrossed to the isogenic *w*<sup>1118</sup> background (BDSC#5905) obtained from Bloomington *Drosophila* Stock Center (BDSC).

For optogenetic experiments, flies were raised in the dark and provided with food supplemented with 0.4 mM ATR (Sigma). ATR was dissolved in absolute ethanol and mixed into the standard fly food. For ATR-negative controls, equivalent amounts of ethanol were mixed in the food.

### Immunohistochemistry staining and confocal imaging

Immunostaining procedures were performed as previously described<sup>71</sup>, with minor modifications. Briefly, 4–5-day-old adult flies were picked and dissected in cold phosphate-buffered saline (PBS). For *trans*-Tango experiments, flies were raised at 18 °C for 15 days. For *retro*-Tango experiments, flies were raised at 25 °C for 15 days. Tissues were then fixed in a 4% paraformaldehyde (PFA) in 0.5% PBS-Triton (PBS-T) solution at room temperature (RT) for 30 min. Samples were then washed in 0.5% PBS-T, four times for 15 min at RT. Next, the

**Table 1 | List of the flies' genotypes used in this study**

Genotype	Source	Description
w1118	BDSC#5905	Control flies in the w- background
QUAS-nuclear localization signal-RFP; <i>trans</i> -Tango	BDSC#95315	<i>trans</i> -Tango with a nuclear reporter
QUAS-nuclear localization signal-RFP; retro-Tango	BDSC#99661 (reporter swapped with the nuclear tagged RFP used in BDSC# 95135)	retro-Tango with a nuclear reporter
Gr64f-Gal4	BDSC#57669	Driver for sweet GRNs <sup>7</sup>
Gr66a-Gal4	BDSC#57670	Driver for bitter GRNs <sup>3</sup>
Gr59c-Gal4	BDSC#57650	Driver for labellar GRNs <sup>76</sup>
Gr23a-Gal4	BDSC#57611	Driver for pharyngeal GRNs <sup>76</sup>
Gr58c-Gal4	BDSC#57646	Driver for leg GRNs <sup>76</sup>
UAS-LK-gRNA	BDSC#81426	Guide RNA for LK
Nos-Gal4; UAS-Cas9	BDSC#67083	Expresses Cas9 in the germline
LKCC9(-Gal4)		Lk mutant <sup>26</sup>
UAS-LKR-gRNA	Dr. Matthias Schlichting	Guide RNA for LKR
LKR CC9(-Gal4)		LkR mutant <sup>26</sup>
Scr-Gal4	BDSC#43655	Driver for SEZ neurons <sup>55</sup>
UAS-LK-RNAi	BDSC#25798	RNAi for LK, generated <sup>77</sup> and validated <sup>28</sup>
LK-p65.AD; ChAT-Gal4.DBD (SELK1)	Generated in this study	Labels the SELKs, the LHLKs (inconsistently), some unidentified SEZ neurons
ChAT-p65.AD; LK-Gal4.DBD (SELK2)	Generated in this study	Labels the SELKs, some neurons in PI, AL, and optical lobe
UAS-IVS-GFP (pJFRC81)	Dr. Michael Texada	GFP reporter under UAS <sup>78</sup>
UAS-LK	Generated in this study	Expresses LK transgene under UAS
UAS-GtACR1	BDSC#92983	Expresses the inhibitory light-gated anion channel under UAS <sup>54</sup>
UAS-CsChrimson-mVenus	BDSC#55135	Expresses the excitatory light-gated cation channel under UAS <sup>48</sup>
LK-Gal4	BDSC#51993	Labels LK neurons (generated by Asahina, K., Anderson, D. (2013.9.23))
Lk-LexA	Generated in this study	Labels LK neurons, some other unidentified neurons in the AVLP, and the optic lobe
LexAop-GFP	BDSC#66687	GFP reporter under LexAop (generated by Baker, B. (2017.1.17))
LexAop-Chrimson-mVenus	BDSC#55138	Expresses the CsChrimson under LexAop (generated by Jayaraman, V. (2014.4.16))
Gr66a-LexA	BDSC#93024	Labels bitter GRNs <sup>79</sup>
UAS-ChAT-RNAi	BDSC#25856	Expresses the RNAi for ChAT under UAS <sup>77,80,81</sup>
UAS-GCaMP6s	BDSC#42746	Expresses the calcium indicator GCaMP6s under UAS (generated by Kim, D. (2013.1.16))
LexAop-CsChrimson-tdTomato	BDSC#82183	Expresses the CsChrimson under LexAop
UAS-SPARC2-S-CsChrimson-tdTomato	BDSC#84145	Stochastic access to neurons
Nsyb-phiC31	BDSC#84152	phiC31 recombinase for the SPARC toolkit

**Table 2 | List of the antibodies used in this study**

Antibody	Source	Concentration
Goat anti-GFP	Rockland (600-101-215)	1:1000
Guinea pig anti-RFP	Susan Brenner-Morton	1:5000
Mouse anti-nc82	DSHB (AB 2314866)	1:20-50
Mouse anti-ChAT4B1	DSHB (AB 528122)	1:100
Rabbit anti-LK	(Nassel et al., 1992)	1:5000
Rabbit anti-ITP	(Hermann-Luibl et al., 2014)	1:5000

tissues were put in 5% heat-inactivated equine or donkey serum (HIES or HIDS) in 0.5% PBS-T for 30 min to 1 h at RT. Subsequently, the samples were transferred to the primary antibody solution in 5% HIES or HIDS in 0.5% PBS-T and stained for 2 overnights at 4 °C. After the primary antibody staining, the samples were washed with 0.5% PBS-T, four times for 15 min at RT, which then were transferred to the

secondary antibody solution in 5% HIES or HIDS in 0.5% PBS-T and stained for another 2 overnights at 4 °C. The secondary antibody solution was washed off with 0.5% PBS-T, four times for 15 min at RT. All the fixing, washing, blocking, and staining steps were carried out on a nutator. The samples were then mounted on a slide (Fisherbrand Superfrost Plus) in Fluoromount-G mounting medium (SouthernBiotech). After curing overnight, the samples were imaged using Zeiss LSM800 confocal microscopy with ZEN software (Zeiss, version 2.1). The acquired images were then processed using the Fiji software (ImageJ, v.2.14.0/1.54f). The list of antibodies used can be found in Table 2.

A representative image out of 4–5 independent brains is shown in the figure panels for the immunohistochemistry experiments.

#### Generation of mutant and transgenic lines

Lk<sup>L3</sup> and Lk<sup>L3-ex3</sup> mutants were generated using CRISPR/Cas9 technology to create double-stranded DNA breaks in the coding sequence. Previously generated gRNA lines targeting the respective genes were

crossed with flies expressing Cas9 in the germ line (see Table 1). The progeny was screened for any deletion mutation in the respective genes using polymerase chain reaction (PCR) and subsequent gel electrophoresis and DNA sequencing. Lines carrying the mutations were selected for and backcrossed for at least 6 generations to the isogenic  $w^{1118}$  background (BDSC#5905).

The vectors for transgenic flies were generated using Gibson Assembly. To clone the plasmids for the split Gal4s, the Lk promoter region (2.2 kbp region upstream of the start codon) was amplified from a Canton S fly genomic DNA using PCR. p65 activation domain and Gal4 DNA binding domain were amplified from commercially available pBPp65ADZpUw (addgene26234) and pBPZpGAL4DBDUw (addgene26233) plasmids, respectively. The ChAT promoter (7.3 kbp region upstream of the start codon) was amplified from the genomic DNA of a Canton S fly. These promoter amplicons were then ligated with split Gal4 coding sequences into the pUASTattB cloning vector using Gibson Assembly.

For the construction of the Lk-LexA plasmid, the LexA.p65 coding sequence was amplified from the pBPnlsLexA::p65Uw vector (Addgene 219858). This coding sequence was ligated together with the Lk promoter amplicon mentioned above using Gibson Assembly in the pUASTattB cloning vector that was linearized via restriction digestion.

To clone UAS-Lk, the coding sequence for the Lk gene was amplified from a PiggyBack vector, DmCD00771608 (PACMAN Resources). The 20XUAS IVS CsChrimson tdtomato\_tr (AddGene111544) plasmid was linearized with XhoI and XbaI restriction digestion enzymes to remove the CsChrimson-tdTomato sequence. The remaining vector backbone was purified with gel extraction which then was used as a template to insert the Lk coding sequence amplicon using Gibson Assembly.

All constructed plasmids were verified via sequencing and used to generate transgenic flies via the PhiC31 system for site-directed genomic integration<sup>72</sup> (Rainbow Transgenic Flies, Inc.). Lk-p65.AD, ChAT-p65.AD and Lk-LexA.p65 constructs were inserted into the atp40 genomic location. Lk-Gal4.DBD and ChAT-Gal4.DBD constructs were inserted into the atp2 genomic location. UAS-Lk construct was inserted into the VK00018 genomic location. Primers used in the generation and confirmation of the fly lines are listed in Table 3.

### flyPAD experiments

4–5-day-old male flies were used. Flies were starved for 21–24 h on a wet Kimwipe before each experiment. Individual flies were mouth-pipetted into each arena and were allowed to feed for an hour in a temperature and humidity-controlled chamber (25 °C, 70% humidity) in the dark.

We used 1 M sucrose for the sweet option and 1 M sucrose mixed with 0.1 mM of lobeline as the bittersweet in two-choice feeding assays. The food substrate was loaded into the wells of the assay in a 1% agarose solution. The data was analyzed using the script provided by the manufacturer (Easy Behavior) in MATLAB. For no-choice experiments, the same food was loaded into both wells of the arena. At the end of the experiment, the number of sips taken from each well in an arena was summed together for each fly. The sip duration data from each well in an arena was averaged for each fly.

### OptoPAD experiments

4–5 days old male flies were starved for 21–24 h on a wet Kimwipe supplemented with 0.4 mM ATR before each experiment. Experiment conditions were the same as the FlyPAD experiments.

For optogenetic activation experiments, one of the food sources was paired with a 2s light activation. The intensity of light used for activation experiments was 15.46  $\mu\text{W mm}^{-2}$  unless otherwise stated. For the optogenetic inhibition experiments, the LEDs were kept on throughout the experiment at a light intensity of 62.38  $\mu\text{W mm}^{-2}$ . For

both types of optogenetic experiments, a green LED was used to minimize the aversion to light.

The preference index (PI) was calculated using the following formula:

$$PI = \frac{\text{Number of sips}_{\text{sweet}} - \text{Number of sips}_{\text{sweet} + \text{light}}}{\text{Number of sips}_{\text{sweet}} + \text{Number of sips}_{\text{sweet} + \text{light}}}$$

### Optogenetic PER experiments

The experimental animals were handled as stated above. Starved flies were cold-anesthetized and mounted on a coverslip using nail polish. Flies were acclimated for at least 30 min in the dark. Green LEDs were at an intensity of 31.23  $\mu\text{W mm}^{-2}$  and used to introduce two light pulses, each lasting 5 s, with a 5-s interval between pulses. Flies' behavior was recorded with a UV-filter camera and scored manually. The PER is scored 1 if the full repertoire of the behavior is observed, 0.5 for the animals that only lifted their rostra and labella, and 0 if the proboscis was not extended at all. The PER scores for the two pulses were averaged per animal, and the average PER score was reported on the graphs.

### Statistical analysis

For the two-choice assays, a pairwise comparison of the total number of sips taken from the sweet substance versus the bittersweet substance at the last time point in the assay was performed, and a t-test was done to test the significance of the difference in feeding from either food source. For no-choice experiments, the number of sips taken by the experimental group was compared to that of the controls in a one-way ANOVA test.

For the two-choice OptoPAD experiments, the data was analyzed in a similar way as the two-choice FlyPAD experiments. When comparing the PIs resulting from the activation of either LK neurons or Gr66a<sup>+</sup> neurons in control and Lk mutant backgrounds in the two-choice OptoPAD paradigm, an unpaired t-test was performed. For the PER experiments, statistical significance was tested with one-way ANOVA when comparing the scores of the experimental groups to the controls'. An unpaired t-test was performed to compare the scores of LK activation in the control and mutant background.

### Transcriptome analysis

We utilized a previously published dataset for the single-cell transcriptome of the adult fly brain<sup>56</sup>. Using a custom R-script, we pooled the cells that highly express Lk (CG13480) transcripts by setting a threshold based on the 99.9th percentile values of LK reads amongst the dataset. We then performed a base-2 logarithmic transformation on the raw read counts to report the relative levels of selected marker gene expression for each cell.

### Connectome analyses and data visualization

SELKs (DN68 cell type) were identified in the female adult fly brain (FAFB), FlyWire connectome<sup>43,46,47</sup>, following manual comparison with light-microscopy staining of a single SELK. We used the v783 snapshot of the FlyWire connectome and its annotations for all the analyses. Neuron reconstructions were visualized using FlyWire neuroglancer<sup>46</sup>. For in silico activation of SELKs, we used the computational brain model and analysis described previously<sup>62</sup> and the Python code publicly provided by Philip Shiu ([https://github.com/philshiu/Drosophila\\_brain\\_model](https://github.com/philshiu/Drosophila_brain_model)). Default parameters used for the model include: -52 mV resting potential and reset potential after spike, -45 mV spiking threshold, 20 ms membrane time scale, 5 ms time constant, 2.2 ms refractory period, 1.8 ms time delay for changes in post-synaptic neuron, and 0.275 mV synaptic weight. SELKs were stimulated for 1 s, and an average of 30 stimulation trials was used. Connectivity and in silico activation analyses were based on updated synapse predictions<sup>73</sup>. All

**Table 3 | List of the primers used in this study**

Primer name	Sequence
Lk promoter_F	TTCGGAAGGGAAGAGCGAG
Lk promoter_R	CTTCTCCAGCGGTTTTAGC
ChAT promoter_	GAGCTCGCCCGGGGATCG
ChAT promoter_R	TTAATTAAGTTTGGTATGCGCTTTGTGATTCAAAGTTGGC
p65.AD_F	ATGGATAAAGCGGAATTAATTCGCCGAGC
p65.AD_R	TTACTTGCCCGCCGCCAG
Gal4.DBD_F	ATGCTGGAGATCCGCGCCGCCT
Gal4.DBD_R	TTACGATACCGTCAGTTG
Lk transgene_F	ATGGCAAAGATAGTCCTGTGTATG
Lk transgene_R	GTAGTCCGCGCAGGATCGG
LexA.p65_F	ATGCCACCCAAGAAGAAG
LexA.p65_R	TTAGGAGCTTATCTGGCTC
LK_genotype_F	GTCTCAGTTTCAAGTGCACGTCACG
LK_genotype_R	TGTAGCCAATGGCTACTAGCCAC
LK_sequencing	GCGACGTGTGTAAACGGCTTAGAAAATGCG
LKRex3_genotype_F	GGGTTGATTAATCATATCAAACCTCAGGC
LKRex3_genotype_R	AGTTGACGTATTGACTTACCGCGAAATC
LKRex3_sequencing	GACGACTCACTGTAGCTATCC

data for figure visualizations were processed and analyzed in R-Studio (2024.04.2 + 764).

### Calcium imaging

4–5 days old male flies were prepared as described previously<sup>16</sup>. Briefly, flies were anesthetized under CO<sub>2</sub>, and all legs were removed to minimize gustatory inputs from these organs. The proboscis was glued out using a UV glue (Loctite). Individual flies were then mounted on the bottom side of a petri dish with a small hole on, upside down. The opposite side of the dish was filled with a ribose artificial hemolymph-like (AHL) solution (108 mM NaCl, 5 mM KCl, 2 mM CaCl<sub>2</sub>, 8.2 mM MgCl<sub>2</sub>, 4 mM NaHCO<sub>3</sub>, 1 mM NaH<sub>2</sub>PO<sub>4</sub>, 15 mM ribose, 5 mM HEPES, pH adjusted to 7.2–7.5, osmolarity adjusted to ~275 mOsm). A window at the base of the proboscis was dissected to expose the SEZ.

A Scientifica multiphoton galvo system was used for two-photon imaging. An excitation wavelength of 920 nm was used. The preparations were imaged with a 16x Nikon objective, and imaging was performed using the SciScan software (Scientifica). Imaging volumes were acquired on 4 planes at a 256 × 256 pixel resolution and at a 6.1 frame/second rate (volume rate ~1.5 Hz).

A Drummond Nanoject II microinjector mounted on a micro-manipulator (Scientifica) was used to administer tastant solutions to the fly proboscis during imaging. In each imaging session, the tastant was manually delivered after collecting at least 10 baseline imaging volumes. A Point Grey Firefly camera equipped with an Infinix lens and a shortpass IR filter (850 nm OD 4.0 shortpass filter, Edmund Optics) was used to monitor the tastant delivery to the proboscis. We used 1 M sucrose for the sweet tastant and 10 mM lobeline as the bitter compound. Each tastant was delivered three times to each fly. The results from the three tastant deliveries were averaged.

For the optogenetic activation, a 635 nm laser that is integrated into the microscope was used at 1 pulse per frame, at an intensity of 7.69 μW mm<sup>-2</sup>. Three experiments were conducted per animal. The results from the three different experiments were averaged per data point.

For the analysis, images were Z-projected at maximum intensity using the Fiji software. The region of interest (ROI) was drawn manually around the cell bodies, and fluorescence levels were measured per frame. A background subtraction was applied. The background

fluorescence was measured from the vicinity of the ROI where there is no apparent fluorescent signal. The area of the background reading was kept identical to that of the ROI, and background fluorescence was subtracted from the actual fluorescence readings of the ROI per time frame.  $\Delta F/F$  was calculated as  $(F-F_0)/F_0$ , where  $F_0$  is the mean value of the ten frames preceding the stimulus presentation.

### Neuropeptide release experiments

Experimental flies were placed in the optoPAD arena. Every 5 min, a green light pulse of 30 s is activated for an hour. At the end of the experiment, flies were collected and dissected immediately. The intensity of light used for activation experiments was 108 μW mm<sup>-2</sup> unless otherwise stated.

### Puncta counting

Puncta were counted as described before<sup>74</sup>. Briefly, images were opened using the Fiji software (ImageJ, v.2.14.o/1.54f). The images were then collapsed on a Z-stack at maximum intensity. Difference of Gaussians were applied using Gaussian radii of 1 and 2. Yielding two images were then subtracted from each other. Using default threshold settings, puncta were analyzed using the “analyze particles” function. For the images obtained with the activation of bitter and sweet GRNs, no size thresholding was applied (Size (pixel<sup>2</sup>) = 0-infinity). For the experiments with the SELK2 driver, a size threshold of 0.35-infinity was applied since these images had to be imaged at a higher gain.

### Corrected total cell fluorescence (CTCF) measurement

CTCF of SELKs is measured to test the efficacy of Lk knockdown as previously described<sup>75</sup>. Briefly, images were collapsed on a Z-stack at maximum intensity on the Fiji software (ImageJ, v.2.14.o/1.54f). An ROI was manually drawn around the cell bodies. The integrated density and area of the ROI were measured on the software. Next, a background was selected, and the mean fluorescence of the background was measured. Finally, CTCF was calculated for each cell using the following formula:

$$CTCF = \text{Integrated density} - (\text{Area} \times \text{mean fluorescence of the background})$$

## Reporting summary

Further information on research design is available in the Nature Portfolio Reporting Summary linked to this article.

## Data availability

The behavioral and functional imaging data generated in this study have been deposited in the Figshare database under accession code <https://doi.org/10.6084/m9.figshare.31049989>. Source data are provided as a Source data file. Source data are provided with this paper.

## Code availability

Custom codes used for data analyses are available at: <https://github.com/Zandawala-lab/Savas-et-al-2025-Drosophila-SELK>.

## References

- Rosenstein, D. & Oster, H. Differential facial responses to four basic tastes in newborns. *Child Dev.* **59**, 1555–1568 (1988).
- Clyne, P. J., Warr, C. G. & Carlson, J. R. Candidate taste receptors in *Drosophila*. *Science* **287**, 1830–1834 (2000).
- Scott, K. et al. A chemosensory gene family encoding candidate gustatory and olfactory receptors in *Drosophila*. *Cell* **104**, 661–673 (2001).
- Accolla, R., Bathellier, B., Petersen, C. C. & Carleton, A. Differential spatial representation of taste modalities in the rat gustatory cortex. *J. Neurosci.* **27**, 1396–1404 (2007).
- Marella, S. et al. Imaging taste responses in the fly brain reveals a functional map of taste category and behavior. *Neuron* **49**, 285–295 (2006).
- Dethier, V. G. *The Hungry Fly: A Physiological Study of the Behavior Associated with Feeding* (Harvard University Press, 1976).
- Dahanukar, A., Lei, Y. T., Kwon, J. Y. & Carlson, J. R. Two Gr genes underlie sugar reception in *Drosophila*. *Neuron* **56**, 503–516 (2007).
- Weiss, L. A., Dahanukar, A., Kwon, J. Y., Banerjee, D. & Carlson, J. R. The molecular and cellular basis of bitter taste in *Drosophila*. *Neuron* **69**, 258–272 (2011).
- Meunier, N., Marion-Poll, F., Rospars, J. P. & Tanimura, T. Peripheral coding of bitter taste in *Drosophila*. *J. Neurobiol.* **56**, 139–152 (2003).
- Inagaki, H. K., Panse, K. M. & Anderson, D. J. Independent, reciprocal neuromodulatory control of sweet and bitter taste sensitivity during starvation in *Drosophila*. *Neuron* **84**, 806–820 (2014).
- Devineni, A. V., Sun, B., Zhukovskaya, A. & Axel, R. Acetic acid activates distinct taste pathways in *Drosophila* to elicit opposing, state-dependent feeding responses. *Elife* **8**, <https://doi.org/10.7554/eLife.47677> (2019).
- Sterne, G. R., Otsuna, H., Dickson, B. J. & Scott, K. Classification and genetic targeting of cell types in the primary taste and premotor center of the adult *Drosophila* brain. *Elife* **10**, <https://doi.org/10.7554/eLife.71679> (2021).
- Shiu, P. K., Sterne, G. R., Engert, S., Dickson, B. J. & Scott, K. Taste quality and hunger interactions in a feeding sensorimotor circuit. *Elife* **11**, <https://doi.org/10.7554/eLife.79887> (2022).
- Scott, K. Gustatory processing in *Drosophila melanogaster*. *Annu. Rev. Entomol.* **63**, 15–30 (2018).
- Kendroud, S. et al. Structure and development of the sub-oesophageal zone of the *Drosophila* brain. II. Sensory compartments. *J. Comp. Neurol.* **526**, 33–58 (2018).
- Snell, N. J. et al. Complex representation of taste quality by second-order gustatory neurons in *Drosophila*. *Curr. Biol.* **32**, 3758–3772 (2022).
- Chu, B., Chui, V., Mann, K. & Gordon, M. D. Presynaptic gain control drives sweet and bitter taste integration in *Drosophila*. *Curr. Biol.* **24**, 1978–1984 (2014).
- Reiter, S., Campillo Rodriguez, C., Sun, K. & Stopfer, M. Spatio-temporal coding of individual chemicals by the gustatory system. *J. Neurosci.* **35**, 12309–12321 (2015).
- Liu, H. & Fontanini, A. State dependency of chemosensory coding in the gustatory thalamus (VPMpc) of alert rats. *J. Neurosci.* **35**, 15479–15491 (2015).
- Sweazey, R. D. & Smith, D. V. Convergence onto hamster medullary taste neurons. *Brain Res.* **408**, 173–184 (1987).
- Nassel, D. R. & Zandawala, M. Recent advances in neuropeptide signaling in *Drosophila*, from genes to physiology and behavior. *Prog. Neurobiol.* **179**, 101607 (2019).
- Marder, E. Neuromodulation of neuronal circuits: back to the future. *Neuron* **76**, 1–11 (2012).
- Bargmann, C. I. & Marder, E. From the connectome to brain function. *Nat. Methods* **10**, 483–490 (2013).
- Cavey, M., Collins, B., Bertet, C. & Blau, J. Circadian rhythms in neuronal activity propagate through output circuits. *Nat. Neurosci.* **19**, 587–595 (2016).
- Yurgel, M. E. et al. A single pair of leucokinin neurons are modulated by feeding state and regulate sleep-metabolism interactions. *PLoS Biol.* **17**, e2006409 (2019).
- Zandawala, M. et al. Modulation of *Drosophila* post-feeding physiology and behavior by the neuropeptide leucokinin. *PLoS Genet.* **14**, e1007767 (2018).
- Nassel, D. R. Substrates for neuronal cotransmission with neuropeptides and small molecule neurotransmitters in *Drosophila*. *Front. Cell. Neurosci.* **12**, 83 (2018).
- Senapati, B. et al. A neural mechanism for deprivation state-specific expression of relevant memories in *Drosophila*. *Nat. Neurosci.* **22**, 2029–2039 (2019).
- Marder, E. & Weimann, J. *Neurobiology of Motor Programme Selection* (Pergamon Press/Elsevier, 1992).
- Huang, Y. C. et al. A single neuron in *C. elegans* orchestrates multiple motor outputs through parallel modes of transmission. *Curr. Biol.* **33**, 4430–4445 (2023).
- Vaaga, C. E., Borisovska, M. & Westbrook, G. L. Dual-transmitter neurons: functional implications of co-release and co-transmission. *Curr. Opin. Neurobiol.* **29**, 25–32 (2014).
- Kim, D.-I. et al. Encoding opposing valences through frequency-dependent transmitter switching in single peptidergic neurons. Preprint at *bioRxiv* <https://doi.org/10.1101/2024.11.09.622790> (2024).
- Talay, M. et al. Transsynaptic mapping of second-order taste neurons in flies by trans-Tango. *Neuron* **96**, 783–795 (2017).
- Snell, N. J., Fisher, J. D., Hartmann, G. G., Talay, M. & Barnea, G. Distributed representation of taste quality by second-order gustatory neurons in *Drosophila*. Preprint at *bioRxiv* <https://doi.org/10.1101/2020.11.10.377382> (2020).
- Nassel, D. R. Leucokinin and associated neuropeptides regulate multiple aspects of physiology and behavior in *Drosophila*. *Int. J. Mol. Sci.* **22**, <https://doi.org/10.3390/ijms22041940> (2021).
- Liu, Y., Luo, J., Carlsson, M. A. & Nassel, D. R. Serotonin and insulin-like peptides modulate leucokinin-producing neurons that affect feeding and water homeostasis in *Drosophila*. *J. Comp. Neurol.* **523**, 1840–1863 (2015).
- Luo, J., Liu, Y. & Nassel, D. R. Insulin/IGF-regulated size scaling of neuroendocrine cells expressing the bHLH transcription factor dimmed in *Drosophila*. *PLoS Genet.* **9**, e1004052 (2013).
- Al-Anzi, B. et al. The leucokinin pathway and its neurons regulate meal size in *Drosophila*. *Curr. Biol.* **20**, 969–978 (2010).
- de Haro, M. et al. Detailed analysis of leucokinin-expressing neurons and their candidate functions in the *Drosophila* nervous system. *Cell Tissue Res.* **339**, 321–336 (2010).
- Zandawala, M., Marley, R., Davies, S. A. & Nassel, D. R. Characterization of a set of abdominal neuroendocrine cells that regulate

- stress physiology using colocalized diuretic peptides in *Drosophila*. *Cell. Mol. Life Sci.* **75**, 1099–1115 (2018).
41. Galikova, M., Dirksen, H. & Nassel, D. R. The thirsty fly: ion transport peptide (ITP) is a novel endocrine regulator of water homeostasis in *Drosophila*. *PLoS Genet.* **14**, e1007618 (2018).
  42. Lopez-Arias, B., Dorado, B. & Herrero, P. Blockade of the release of the neuropeptide leucokinin to determine its possible functions in fly behavior: chemoreception assays. *Peptides* **32**, 545–552 (2011).
  43. Zheng, Z. et al. A complete electron microscopy volume of the brain of adult *Drosophila melanogaster*. *Cell* **174**, 730–743 e722 (2018).
  44. Isaacman-Beck, J. et al. SPARC enables genetic manipulation of precise proportions of cells. *Nat. Neurosci.* **23**, 1168–1175 (2020).
  45. Matsliah, A. et al. *Codex: Connectome Data Explorer*. <https://doi.org/10.13140/RG.2.2.35928.67844> (2023).
  46. Dorkenwald, S. et al. Neuronal wiring diagram of an adult brain. *Nature* **634**, 124–138 (2024).
  47. Schlegel, P. et al. Whole-brain annotation and multi-connectome cell typing of *Drosophila*. *Nature* **634**, 139–152 (2024).
  48. Klapoetke, N. C. et al. Independent optical excitation of distinct neural populations. *Nat. Methods* **11**, 338–346 (2014).
  49. Chen, T. W. et al. Ultrasensitive fluorescent proteins for imaging neuronal activity. *Nature* **499**, 295–300 (2013).
  50. Inagaki, H. K. et al. Visualizing neuromodulation in vivo: TANGO-mapping of dopamine signaling reveals appetite control of sugar sensing. *Cell* **148**, 583–595 (2012).
  51. Marella, S., Mann, K. & Scott, K. Dopaminergic modulation of sucrose acceptance behavior in *Drosophila*. *Neuron* **73**, 941–950 (2012).
  52. Sareen, P. F., McCurdy, L. Y. & Nitabach, M. N. A neuronal ensemble encoding adaptive choice during sensory conflict in *Drosophila*. *Nat. Commun.* **12**, 4131 (2021).
  53. Moreira, J. M. et al. optoPAD, a closed-loop optogenetics system to study the circuit basis of feeding behaviors. *Elife* **8**, <https://doi.org/10.7554/eLife.43924> (2019).
  54. Mohammad, F. et al. Optogenetic inhibition of behavior with anion channelrhodopsins. *Nat. Methods* **14**, 271–274 (2017).
  55. Simpson, J. H. Rationally subdividing the fly nervous system with versatile expression reagents. *J. Neurogenet.* **30**, 185–194 (2016).
  56. Davie, K. et al. A single-cell transcriptome atlas of the aging *Drosophila* brain. *Cell* **174**, 982–998 (2018).
  57. Kahsai, L., Kapan, N., Dirksen, H., Winther, A. M. & Nassel, D. R. Metabolic stress responses in *Drosophila* are modulated by brain neurosecretory cells that produce multiple neuropeptides. *PLoS ONE* **5**, e11480 (2010).
  58. Herrero, P., Magarinos, M., Torroja, L. & Canal, I. Neurosecretory identity conferred by the apterous gene: lateral horn leucokinin neurons in *Drosophila*. *J. Comp. Neurol.* **457**, 123–132 (2003).
  59. Kitamoto, T. & Salvaterra, P. M. A POU homeo domain protein related to dPOU-19/pdm-1 binds to the regulatory DNA necessary for vital expression of the *Drosophila* choline acetyltransferase gene. *J. Neurosci.* **15**, 3509–3518 (1995).
  60. Hamid, R. et al. *Drosophila* choline transporter non-canonically regulates pupal eclosion and NMJ integrity through a neuronal subset of mushroom body. *Dev. Biol.* **446**, 80–93 (2019).
  61. Dethier, V. G. Other tastes, other worlds. *Science* **201**, 224–228 (1978).
  62. Shiu, P. K. et al. A *Drosophila* computational brain model reveals sensorimotor processing. *Nature* **634**, 210–219 (2024).
  63. Sorkac, A. et al. retro-Tango enables versatile retrograde circuit tracing in *Drosophila*. *Elife* **12**, <https://doi.org/10.7554/eLife.85041> (2023).
  64. Chanat, E. & Huttner, W. B. Milieu-induced, selective aggregation of regulated secretory proteins in the trans-Golgi network. *J. Cell Biol.* **115**, 1505–1519 (1991).
  65. Nordmann, J. J. & Morris, J. F. Method for quantitating the molecular content of a subcellular organelle: hormone and neurophysin content of newly formed and aged neurosecretory granules. *Proc. Natl. Acad. Sci. USA* **81**, 180–184 (1984).
  66. Karhunen, T., Vilim, F. S., Alexeeva, V., Weiss, K. R. & Church, P. J. Targeting of peptidergic vesicles in cotransmitting terminals. *J. Neurosci.* **21**, RC127 (2001).
  67. Molla-Albaladejo, R., Jimenez-Caballero, M. & Sanchez-Alcaniz, J. A. Molecular characterization of gustatory second-order neurons reveals integrative mechanisms of gustatory and metabolic information. *Elife* **13**, <https://doi.org/10.7554/eLife.100947> (2025).
  68. Ohla, K. et al. Recognizing taste: coding patterns along the neural axis in mammals. *Chem. Senses* **44**, 237–247 (2019).
  69. Pfaffmann, C. The afferent code for sensory quality. *Am. Psychol.* **14**, 226 (1959).
  70. Kvello, P., Jorgensen, K. & Mustaparta, H. Central gustatory neurons integrate taste quality information from four appendages in the moth *Heliothis virescens*. *J. Neurophysiol.* **103**, 2965–2981 (2010).
  71. Wu, J. S. & Luo, L. A protocol for dissecting *Drosophila melanogaster* brains for live imaging or immunostaining. *Nat. Protoc.* **1**, 2110–2115 (2006).
  72. Groth, A. C., Fish, M., Nusse, R. & Calos, M. P. Construction of transgenic *Drosophila* by using the site-specific integrase from phage phiC31. *Genetics* **166**, 1775–1782 (2004).
  73. Yu, S.-C. et al. New synapse detection in the whole-brain connectome of *Drosophila*. Preprint at *bioRxiv* <https://doi.org/10.1101/2025.07.11.664377> (2025).
  74. Iwabuchi, S., Kakazu, Y., Koh, J. Y. & Harata, N. C. Evaluation of the effectiveness of Gaussian filtering in distinguishing punctate synaptic signals from background noise during image analysis. *J. Neurosci. Methods* **223**, 92–113 (2014).
  75. The Open Lab Book. *Measuring cell fluorescence using ImageJ* <https://theolb.readthedocs.io/en/latest/imaging/measuring-cell-fluorescence-using-imagej.html> (2014).
  76. Kwon, J. Y., Dahanukar, A., Weiss, L. A. & Carlson, J. R. A map of taste neuron projections in the *Drosophila* CNS. *J. Biosci.* **39**, 565–574 (2014).
  77. Perkins, L. A. et al. The transgenic RNAi project at Harvard Medical School: resources and validation. *Genetics* **201**, 843–852 (2015).
  78. Pfeiffer, B. D., Truman, J. W. & Rubin, G. M. Using translational enhancers to increase transgene expression in *Drosophila*. *Proc. Natl. Acad. Sci. USA* **109**, 6626–6631 (2012).
  79. Thistle, R., Cameron, P., Ghorayshi, A., Dennison, L. & Scott, K. Contact chemoreceptors mediate male-male repulsion and male-female attraction during *Drosophila* courtship. *Cell* **149**, 1140–1151 (2012).
  80. Ishimoto, H. & Kamikouchi, A. A feedforward circuit regulates action selection of pre-mating courtship behavior in female *Drosophila*. *Curr. Biol.* **30**, 396–407 (2020).
  81. Itskov, P. M. et al. Automated monitoring and quantitative analysis of feeding behaviour in *Drosophila*. *Nat. Commun.* **5**, 4560 (2014).

## Acknowledgements

This work was supported by NIH grant R01DC020703 (G.B.), Brown University Carney Institute for Brain Science, Suna Kırac Fund for Brain Science (D.S.), Brown University Carney Institute for Brain Science, Graduate Award in Brain Science (D.S.) and NIH/NIDCD award F31DC019540 (A.M.C.). Stocks obtained from the Bloomington *Drosophila* Stock Center (NIH P40OD018537) were used in this study. We thank Dr. Brian Kim for conducting preliminary behavioral studies. We thank Susan Brenner-Morton and Drs. Dick Nässel and Matthias Schlichting for sharing reagents. We would like to thank Drs. Karla Kaun, Alexander Fleischmann, Mustafa Talay, and members of the Barnea Laboratory for critical reading of the manuscript.

## Author contributions

D.S., M.Z., and G.B. conceptualized the study. D.S., A.O., R.A.M., A.M.C., Z.C., R.S., A.S., and M.Z. contributed to the acquisition and analysis of the data. D.S. and G.B. administered the project. D.S. and G.B. wrote the manuscript. The project was supervised by M.Z. and G.B.

## Competing interests

The authors declare no competing interests.

## Additional information

**Supplementary information** The online version contains Supplementary material available at <https://doi.org/10.1038/s41467-026-69443-8>.

**Correspondence** and requests for materials should be addressed to Gilad Barnea.

**Peer review information** *Nature Communications* thanks the anonymous reviewers for their contribution to the peer review of this work. A peer review file is available.

**Reprints and permissions information** is available at <http://www.nature.com/reprints>

**Publisher's note** Springer Nature remains neutral with regard to jurisdictional claims in published maps and institutional affiliations.

**Open Access** This article is licensed under a Creative Commons Attribution-NonCommercial-NoDerivatives 4.0 International License, which permits any non-commercial use, sharing, distribution and reproduction in any medium or format, as long as you give appropriate credit to the original author(s) and the source, provide a link to the Creative Commons licence, and indicate if you modified the licensed material. You do not have permission under this licence to share adapted material derived from this article or parts of it. The images or other third party material in this article are included in the article's Creative Commons licence, unless indicated otherwise in a credit line to the material. If material is not included in the article's Creative Commons licence and your intended use is not permitted by statutory regulation or exceeds the permitted use, you will need to obtain permission directly from the copyright holder. To view a copy of this licence, visit <http://creativecommons.org/licenses/by-nc-nd/4.0/>.

© The Author(s) 2026